J. Fluid Mech. (2004), *vol.* 517, *pp.* 251–279.
DOI: 10.1017/S002211200400093X Printed in the United Kingdom

Thermo-mechanical instabilities in Dean and Taylor–Couette flows: mechanisms and scaling laws

By D. G. THOMAS, R. SURESHKUMAR† AND B. KHOMAMI

Department of Chemical Engineering, Washington University, St. Louis, MO 63130, USA

(Received 6 February 2003 and in revised form 14 May 2004)

The influence of fluid thermal sensitivity on the centrifugal flow instabilities in pressure-driven (Dean) and drag-driven (Taylor–Couette) Newtonian shear flows is investigated. Thermal effects are caused by viscous heating or an externally imposed temperature difference between the outer and inner cylinders, ΔT^*, or a combination of both. In all cases considered, the maximum temperature difference within the gap is small enough such that the base-state velocity profile and consequently the distribution of angular momentum are practically unchanged from those in the isothermal flow. The base-state temperature gradient can be approximated as a linear superposition of $\Delta T^*/d$, where d is the gap width, and that caused by viscous heating. Numerical linear stability analysis shows that when $\Delta T^* = 0$, viscous heating causes the critical Reynolds number, Re_c, to be greatly reduced when the Nahme number, defined as the product of the Brinkman number, Br, and the dimensionless activation energy associated with the fluid viscosity, ε, is $O(\alpha^2/Pr)$ where α and Pr denote the dimensionless critical axial wavenumber and Prandtl number respectively. Since α^2 is $O(10)$ and typical Pr values for thermal sensitive liquids could be $O(10^4)$, appreciable flow destabilization occurs even when Na is $O(10^{-3})$. In the absence of viscous heating, an externally imposed temperature gradient can lead to significant reduction in Re_c when $S \equiv (\varepsilon \Delta T^*)/T_1^* < 0$ and $|S|$ is $O(\alpha^2/Pr)$, where T_1^* denotes the temperature of the inner cylinder. The numerical linear stability analysis results are explained based on a simplified model derived from the linearized governing equations by invoking the narrow-gap approximation. This model shows that the thermo-mechanical coupling, arising from the convection of the base-state temperature gradient by radial velocity perturbation, amplifies the temperature fluctuations within the flow by a factor proportional to Pe/α^2 where Pe denotes the Péclet number. This results in the reduction of local viscosity. Hence, the rate of dissipation of the velocity perturbations decreases causing the centrifugal instability to occur at lower values of the Reynolds number compared to the isothermal flow. Thermo-mechanical destabilization caused by viscous heating for $\Delta T^* = 0$ can be quantified by a scaling law of the form $\Lambda = [1 + Pr\, c_1\ Na/\alpha^2]^{-1/2}$ where Λ is the ratio of the critical Reynolds number of the non-isothermal flow to that of the isothermal one and c_1 is a flow-dependent constant. Similarly, in the absence of viscous heating and for $\Delta T^* < 0$, $\Lambda = [1 + Prc_2 S/\alpha^2]^{-1/2}$, where c_2 is a flow-dependent constant. When $\Delta T^* > 0$ and viscous heating are present, a numerical linear stability analysis shows that $\Lambda \propto Na^k$ where $k < 0$ and it is dependent on ΔT^* and the flow type. Finally, we perform a nonlinear stability analysis

† Author to whom correspondence should be addressed: suresh@wuche.wustl.edu

for the Dean flow which shows that the bifurcation is supercritical for both stationary and time-dependent modes of instability.

1. Introduction

We present a theoretical investigation of the effect of temperature-dependent fluid viscosity on the stability of curvilinear shear flows of Newtonian fluids confined between two infinitely long concentric cylinders driven by either a constant azimuthal pressure gradient or relative rotation of the cylinders. It has long been established that centrifugal instabilities occur in such flows: Taylor (1923) first considered drag-driven flow between two coaxial cylinders (Taylor–Couette flow) and later Dean (1928) first studied viscous flow through a curved channel driven by a streamwise pressure gradient (Dean flow). As reported by Taylor (1923) and Dean (1928), in the limit of narrow gaps, the unidirectional base flow becomes unstable when $Re_c(d/R_1)^{1/2}$ exceeds a critical value of 41 and 36 for Taylor–Couette and Dean flows respectively, where Re_c denotes the critical Reynolds number, d is gap width and R_1 is the radius of the inner cylinder.

Recently, Al-Mubaiyedh, Sureshkumar & Khomami (1999, 2002) performed a stability analysis to ascertain the role of thermal effects induced by viscous dissipation on the Taylor–Couette flow instability. Their work focused on liquids that possess (*a*) high viscosity ($O(1)$ Pa s) at room temperature and (*b*) large activation energy ($O(10^2)$ kJ mole^{-1}) associated with the (Arrhenius) temperature dependence of viscosity (e.g. glycerin, glycerin/water mixture, polydimethylsiloxane oligomers). An appropriate measure of the thermal sensitivity of the fluid is the Nahme–Griffith number, *Na*, which is the ratio of the temperature rise due to viscous heating to the temperature rise necessary to make an $O(1)$ change in the viscosity. It can be related to the Brinkman number, *Br*, via the dimensionless activation energy associated with the fluid viscosity, ε, as $Na = \varepsilon Br$. By definition, *Br* represents the ratio of the rates of viscous heating to conduction. Al-Mubaiyedh *et al.* (1999, 2002) predicted that even temperature non-homogeneities as small as 1–2 K within the gap, generated by viscous heating, could lead to dramatic destabilization of the flow, e.g. the critical Reynolds number in the presence of thermal effects could be an order of magnitude smaller than the isothermal one. In addition, the temporal characteristics of the secondary flow were found to depend on the thermal boundary conditions imposed. White & Muller (2000, 2002*a*) have performed flow visualization experiments to investigate the effect of viscous heating on the stability of Taylor–Couette flow of viscous thermally sensitive liquids. Their experimental observations have corroborated the theoretical predictions of Al-Mubaiyedh *et al.* (1999, 2002). Theoretical predictions of the critical Reynolds number are within 40% of the experimentally reported ones (Thomas, Sureshkumar & Khomami 2003). Since the temperature variations within the gap are small ($\sim$1 K), typical values of the Grashof number are $\ll 1$. Hence, buoyancy effects are neglected in this analysis.

For Taylor–Couette flow, Al-Mubaiyedh *et al.* (2002) performed detailed analyses of the influence of thermal effects on the steady-state pressure distribution and kinematics as well as the unstable eigendisturbances to understand qualitatively the mechanism of the flow destabilization caused by viscous heating. They found that the coupling between velocity perturbations and the base-state temperature gradient can give rise to spatially non-homogeneous temperature fluctuations within the gap. For

thermally sensitive fluids, such thermal fluctuations could reduce the local viscosity leading to decreased dissipation of velocity disturbances. This results in the loss of stability of the base Couette flow.

While the onset and nonlinear evolution of thermo-mechanical instabilities in Taylor–Couette flow have been established by experimental and theoretical investigations (e.g. White & Muller 2000, 2002*a*, *b*; Al-Mubaiyedh *et al.* 2002; Thomas *et al.* 2003), a quantitative model for the thermo-mechanical coupling that causes the observed instabilities has not yet been developed. For instance, Nahme number values at which the thermal effects start to have an appreciable effect on flow stability are much smaller than unity, e.g. refer to figures 1(*a*) and 1(*b*) in Al-Mubaiyedh *et al.* (2002) which show that Re_c is significantly reduced even when $10^{-2} < Na < 10^{-1}$. Although an empirical form for the Re_c–Na_c relationship has been suggested based on experimental data and numerical linear stability analysis (White & Muller 2002*b*; Thomas *et al.* 2003), the precise mechanism by which the Prandtl number, Pr, and the axial wavenumber of the critical disturbance, α, influence the Re_c–Na_c relationship is unknown. In addition, even in the absence of viscous heating, externally imposed temperature gradients could influence flow stability if the fluid is thermally sensitive. It is not clear how an external temperature gradient influences Re_c when viscous heating plays a negligible role in determining the thermal profile. Moreover, it is not known whether similar instabilities exist in other types of flows that have served as classical paradigms of stability and nonlinear hydrodynamics. Especially of interest is Dean flow (Dean 1928), which has been used as a model for pressure-driven flow through curved channels. Note that Taylor–Couette flow is drag-driven, i.e. it is generated by the relative rotation of the cylinders. Hence, explicit external forcing by a pressure gradient is absent. Therefore, it is instructive to examine whether the thermo-mechanical instabilities observed in Taylor–Couette flow also exist in pressure-driven flows. Based on the above-mentioned motivations, we perform stability analysis of Dean and Taylor–Couette flows with the objective of developing a quantitative mechanistic understanding of thermo-mechanical coupling in curvilinear shear flows of Newtonian liquids. Based on approximate analytical solutions valid in the narrow-gap limit for the base state, a simplified model that relates Re, Na, Pr and α at critical conditions is derived. This model is used to explain the predictions of the numerical stability analysis and develop scaling laws that relate Re_c and Na_c. We also perform a nonlinear stability analysis for Dean flow to determine the evolution of finite-amplitude disturbances for $Re > Re_c$. These results are compared with analogous ones for Taylor–Couette flow.

This paper is organized as follows. Problem formulation, dimensionless parameters and solution procedure are presented in § 2. Results and discussion are presented in § 3. Specifically, the analysis of the base state is presented in § 3.1, numerical linear stability analysis results in § 3.2, a discussion of the mechanism and scaling law in § 3.3 and nonlinear stability analysis in § 3.4. In § 4, we present our conclusions. Appendix C contains the details of the derivation of the scaling laws.

2. Problem formulation, dimensionless parameters and solution procedure

We consider the flow of a highly viscous Newtonian fluid confined between two stationary coaxial infinitely long cylinders of radii R_1 and R_2, where subscripts 1 and 2 correspond to the inner and outer cylinders respectively. Dean flow is driven by a constant azimuthal pressure gradient, G^*. The equations governing the base flow are non-dimensionalized using $d = R_2 - R_1$, average steady-state velocity V, d/V, ρV^2 as

the respective length, velocity, time and pressure scales, where ρ denotes the fluid density. Note that V is $O(\sqrt{G^*/\rho})$. It is computed *a posteriori* from the steady-state solution. For Taylor–Couette flow, V is the velocity of the rotating inner cylinder consistent with our earlier work (Al-Mubaiyedh *et al.* 2002). The dimensionless temperature, T, is scaled with respect to a reference temperature T_0^* which is taken to be equal to the inner cylinder temperature T_1^*. Specifically, we set $T_0^* = T_1^* = 298.15\,\mathrm{K}$.

The dimensionless equation of continuity for an incompressible fluid is given by

$$\nabla \cdot \boldsymbol{u} = 0. \tag{1}$$

In dimensionless form, the equation of motion is given by

$$\left[\frac{\partial \boldsymbol{u}}{\partial t} + \boldsymbol{u}\cdot\nabla\boldsymbol{u}\right] = -\nabla p + l_K \frac{1}{r\delta}\hat{e}_\theta + \frac{1}{Re}\nabla\cdot\left[\mathrm{e}^{\varepsilon(1/T-1)}\boldsymbol{\kappa}\right], \tag{2}$$

where $\boldsymbol{\kappa} \equiv \nabla\boldsymbol{u} + \nabla\boldsymbol{u}^t$, the Reynolds number $Re \equiv \rho V d/\eta_0$, p is the hydrodynamic pressure, $\delta \equiv d/R_1$, l_K is 1 or 0 for Dean or Taylor–Couette flows respectively. The fluid viscosity is related to the temperature through an Arrhenius relationship with ε representing the dimensionless activation energy given by $\Delta H/RT_0^*$, where ΔH and R are the dimensional activation energy and the universal gas constant respectively. The dimensionless energy equation can be written as

$$Pe\left[\frac{\partial T}{\partial t} + \boldsymbol{u}\cdot\nabla T\right] = \nabla^2 T + \frac{Br}{2}\mathrm{e}^{\varepsilon(1/T-1)}\boldsymbol{\kappa}:\boldsymbol{\kappa}, \tag{3}$$

where the Brinkman number, $Br \equiv \eta_0 V^2/kT_0^*$, and the Péclet number $Pe \equiv Re\,Pr$. Pr is the Prandtl number defined as $Pr \equiv \eta_0 C_p/k$, where C_p and k are the specific heat capacity at constant pressure and thermal conductivity of the fluid respectively evaluated at T_0^*. The Nahme–Griffith number is defined as $Na \equiv |\partial\eta/\partial T^*|_{T_0^*} V^2/k = \varepsilon\, Br$. In the above governing equations, we have neglected buoyancy effects, since the Grashof number, representing the ratio of buoyancy to viscous forces, is less than 0.02 in the parameter range considered in this study.

The base-flow momentum and energy equations can be expressed as

$$l_K\frac{1}{r\delta} + \mathrm{e}^{\varepsilon(1/T-1)}\left[\frac{\mathrm{d}}{\mathrm{d}r}\left(\frac{1}{r}\frac{\mathrm{d}}{\mathrm{d}r}(ru_\theta)\right) - \frac{\varepsilon}{T^2}r\frac{\mathrm{d}}{\mathrm{d}r}\left(\frac{u_\theta}{r}\right)\frac{\mathrm{d}T}{\mathrm{d}r}\right] = 0, \tag{4}$$

$$\frac{1}{r}\frac{\mathrm{d}}{\mathrm{d}r}\left(r\frac{\mathrm{d}T}{\mathrm{d}r}\right) + Br\,\mathrm{e}^{\varepsilon(1/T-1)}\left[r\frac{\mathrm{d}}{\mathrm{d}r}\left(\frac{u_\theta}{r}\right)\right]^2 = 0. \tag{5}$$

A steady-state solution can be obtained using perturbation analysis numerically by solving equations (4) and (5), along with no-slip boundary conditions for azimuthal velocity and Dirichlet boundary conditions for temperature at the cylinder walls (see § 3.1). Chebyshev spectral collocation method has been used to obtain a numerical solution (Al-Mubaiyedh *et al.* 2002). Linear stability analysis is based on the classical normal-mode perturbation analysis, where infinitesimally small disturbances with axial wavenumber, α, and azimuthal wavenumber, ξ, are superimposed onto the base solution, i.e. $\boldsymbol{X} = \boldsymbol{X}_{ss} + \mathrm{Re}\,[\hat{\boldsymbol{X}}(r)\,\mathrm{e}^{\mathrm{i}\xi\theta+\mathrm{i}\alpha z+\sigma t}]$, where $\boldsymbol{X}$ represents the vector of dependent variables $(p, u_r, u_\theta, u_z, T)$, $\boldsymbol{X}_{ss}(u_{\theta ss}, T_{ss})$ represents the steady-state solution, $\hat{\boldsymbol{X}}(r)$ denotes the radial dependence of the perturbation and $\sigma = \sigma_R + \mathrm{i}\sigma_I$ denotes the corresponding eigenvalues. Substitution of the normal-mode expansion in equations (1), (2) and (3), and the boundary conditions, and further linearization about the base state, leads to a complex differential eigenvalue problem (DEVP). We use the

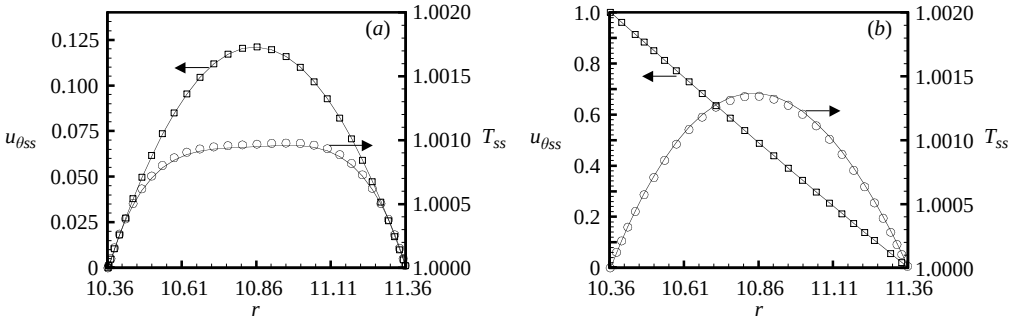

FIGURE 1. Comparison between perturbation series solution (solid line) and numerical results (symbols) for base state. (*a*) Dean flow ($Na = 0.02$), (*b*) Taylor–Couette flow ($Na = 0.25$). $R_1/R_2 = 0.912$, $\Delta T^* = 0$. $Pr = 7975.16$.

Chebyshev collocation technique to reduce the DEVP to a generalized algebraic eigenvalue problem of the type $\boldsymbol{A}\hat{\boldsymbol{X}} = \sigma \boldsymbol{B}\hat{\boldsymbol{X}}$ (Al-Mubaiyedh *et al.* 2002).

3. Results and discussion

3.1. *Base-flow solution*

In this section, analytical solutions for the steady-state velocity and temperature profiles in Dean and Taylor–Couette flows are presented in the form of a regular perturbation series for small values of Br ($Br \ll 1$). Similar methods have been used in the literature to obtain asymptotic base-state solutions in the presence of viscous heating (e.g. Papathanasiou 1997) for the Taylor–Couette flow with stationary inner and rotating outer cylinders. In the case of Dean flow, for $\Delta T^* = 0$, the solutions to first-order accuracy in $Br = Na/\varepsilon$ are given by

$$u_{\theta ss} = u_0 + \frac{Na}{\varepsilon} u_1 + O\left(\left(\frac{Na}{\varepsilon}\right)^2\right), \tag{6}$$

$$\theta_{ss} \equiv \frac{T^*_{ss} - T^*_0}{T^*_0} = \theta_0 + \frac{Na}{\varepsilon}\theta_1 + O\left(\left(\frac{Na}{\varepsilon}\right)^2\right), \tag{7}$$

$$u_0 = -\frac{C_1}{2r} - \frac{r \ln r}{2\delta} + C_2 r, \tag{8}$$

$$u_1 = \frac{\varepsilon C_1^3}{16r^3} - \frac{\varepsilon(C_1C_3 + 2C_1C_4 + 2C_5 + 2C_1C_3 \ln r)}{4r} - \frac{\varepsilon\left(3C_1^2 + 4C_1^2 \ln r + 4C_1^2(\ln r)^2\right)}{16\delta r}$$
$$- \frac{\varepsilon C_1 r(3 \ln r + 4(\ln r)^3)}{48\delta^2} - \frac{\varepsilon r(2C_4 \ln r + C_3(\ln r)^2)}{4\delta} + \frac{\varepsilon r^3}{64\delta^3} + \varepsilon C_6 r, \tag{9}$$

$$\theta_0 = 0, \tag{10}$$

$$\theta_1 = -\frac{C_1^2}{4r^2} + \frac{C_1(\ln r)^2}{2\delta} - \frac{r^2}{16\delta^2} + C_3 \ln r + C_4, \tag{11}$$

where C_1, C_2, C_3, C_4, C_5 and C_6 are given in Appendix A. The subscript '*ss*' denotes steady state. The above series solution compares well with the numerical one up to $Na \approx 0.02$ as shown in figure 1(*a*). While the first-order solution for the velocity is a good approximation, higher-order terms need to be included in order to obtain a better comparison for the temperature for $Na > 0.02$. We have not performed such

an analysis as the range $0 < Na \leqslant 0.02$ spans a major portion of the Na-space where significant reduction in the critical Reynolds number is predicted (see § 3.2).

By employing a similar approach, a series solution for Taylor–Couette flow for $\Delta T^* = 0$ can be expressed in terms of equations (6) and (7) with ($\zeta \equiv R_1/R_2$):

$$u_0 = \frac{(\zeta^2\delta^2 r^2 - 1)}{(\zeta^2 - 1)\delta^2 r}, \tag{12}$$

$$u_1 = \frac{\varepsilon}{2(\zeta^2-1)^3\delta^4 r^3} + \left(\frac{2}{(\zeta^2-1)^2} - 2A - \frac{4}{(\zeta^2-1)^3}\right)\left(\frac{\varepsilon}{4\delta^2 r \ln\zeta}\right) + \frac{\varepsilon \ln(r\delta)}{(\zeta^2-1)^2\delta^2 r \ln\zeta} + \varepsilon Br, \tag{13}$$

$$\theta_0 = 0, \tag{14}$$

$$\theta_1 = \frac{(\delta^2 r^2 - 1)}{(\zeta^2 - 1)^2\delta^2 r^2} - \frac{\ln(r\delta)}{(\zeta^2 - 1)\ln\zeta}, \tag{15}$$

where A, B are given in Appendix A. The analytical series solution compares well with the numerical solution as shown in figure 1(b). For $Na > 0.25$, higher-order terms are required to obtain an accurate solution for the temperature while a first-order solution is a good approximation for the velocity for $Na \leqslant 1$.

Similar perturbation solutions can be obtained for non-zero values of ΔT^* as well. However, as evident from equations (6)–(15), the analytical forms of $u_{\theta ss}$ and θ_{ss} cannot be used in a straightforward manner to perform a linear stability analysis. Hence, subject to *a posteriori* validation by comparison with numerical results, we use the following expressions for the steady-state profiles required in the approximate linear stability analysis presented for narrow gaps in § 3.3:

$$u_{\theta ss} \approx u_{\theta,iso} = \begin{cases} x(1-x) & \text{(Dean)}, \\ 1 - x & \text{(Taylor–Couette)}, \end{cases} \tag{16}$$

where $x \equiv r - r_1$, $0 \leqslant x \leqslant 1$ and $r_1 \equiv R_1/d$.

It is evident from figures 2 and 3 that the temperature profile consists of two contributions, one due to the externally imposed gradient ΔT and the other caused by viscous heating alone with $\Delta T = 0$. The steady-state energy equation has the following form in the narrow-gap limit:

$$\frac{\mathrm{d}^2 T_{ss}}{\mathrm{d}x^2} = -Br\left[\frac{-u_{\theta ss}}{x} + \frac{\mathrm{d}u_{\theta ss}}{\mathrm{d}x}\right]^2. \tag{17}$$

For $Br \ll 1$, the right-hand side can be treated as a source term. Hence,

$$T_{ss} = T_h(x) + T_p(x), \tag{18}$$

where $T_h(x)$ and $T_p(x)$ are the homogeneous and particular solutions respectively such that $T_p(x) = 0$ at $x = 0$ and 1. This decomposition gives

$$T_h(x) = 1 + \Delta T x. \tag{19}$$

Further, by comparing equations (7), (18) and (19), $T_p(x)$ should be given by the narrow-gap approximation of θ_1. As shown in Appendix C or § 3.3, the specific form of $T_p(x)$ is not required for deriving scaling laws between Re_c and Na_c. Hence, we let

$$T_p(x) = \frac{Na}{\varepsilon} g(x). \tag{20}$$

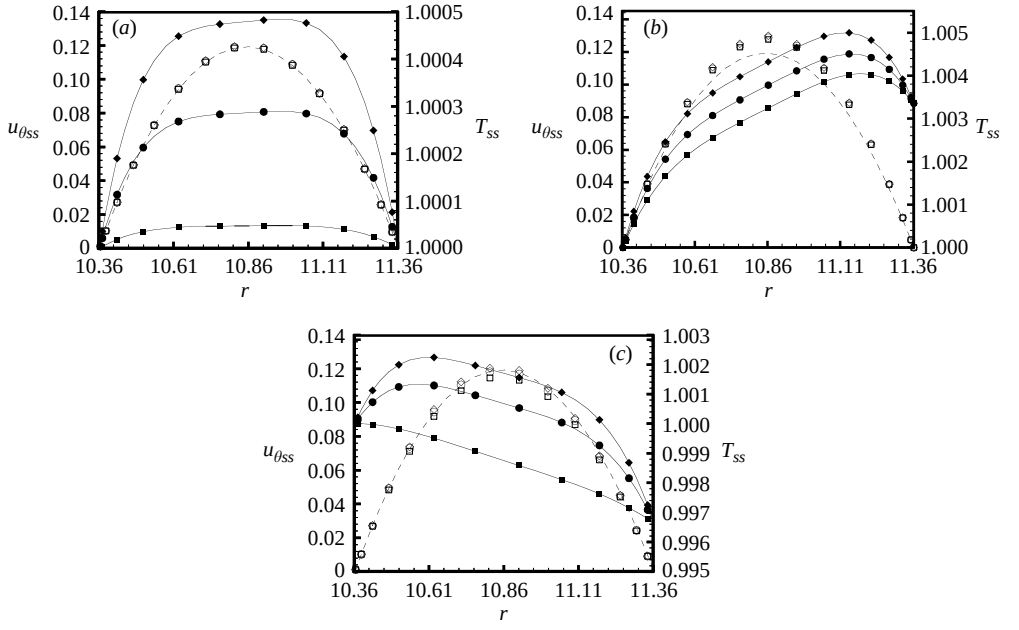

FIGURE 2. Steady-state solution for Dean flow, $u_{\theta ss}$ (open symbols) and T_{ss} (closed symbols). (*a*) $\Delta T^* = 0$: ■, □, $Na = 0.002$; ●, ○, $Na = 0.011$; ◆, ◇, $Na = 0.018$. (*b*) $\Delta T^* = 1\,\mathrm{K}$: ■, □, $Na = 0.061$; ●, ○, $Na = 0.082$; ◆, ◇, $Na = 0.104$. (*c*) $\Delta T^* = -1\,\mathrm{K}$: ■, □, $Na = 0.016$; ●, ○, $Na = 0.087$; ◆, ◇, $Na = 0.125$. Dashed line represents the isothermal steady-state velocity. $R_1/R_2 = 0.912$, $Pr = 7975.16$.

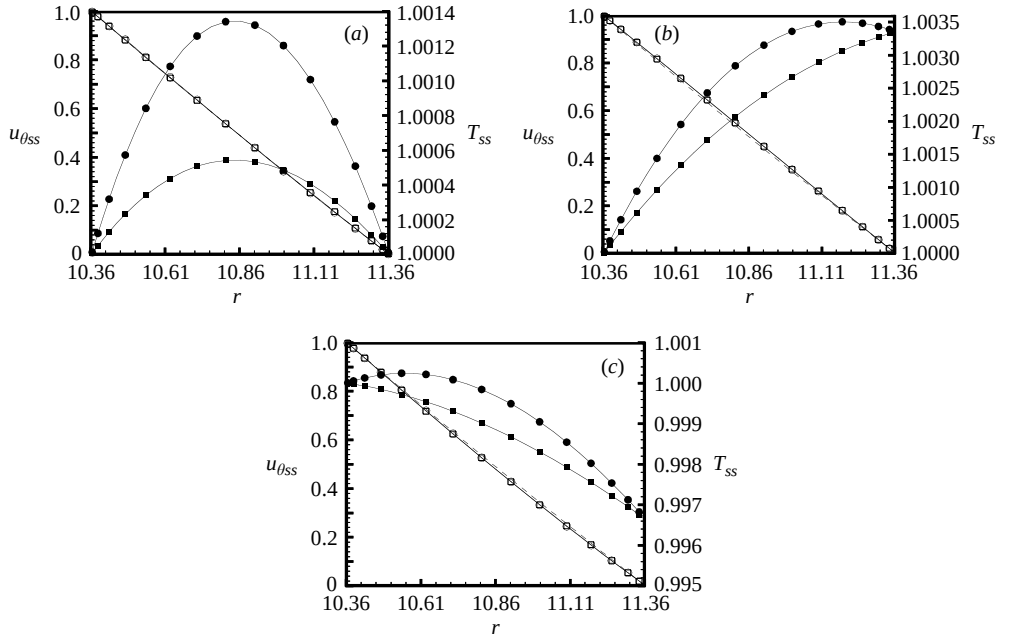

FIGURE 3. Steady-state solution for Taylor–Couette flow, $u_{\theta ss}$ (open symbols) and T_{ss} (closed symbols) at ■, □, $Na = 0.249$ and ●, ○, $Na = 0.1$. (*a*) $\Delta T^* = 0$. (*b*) $\Delta T^* = 1\,\mathrm{K}$. (*c*) $\Delta T^* = -1\mathrm{K}$. Dashed line represents the isothermal steady-state velocity. $R_1/R_2 = 0.912$, $Pr = 7975.16$.

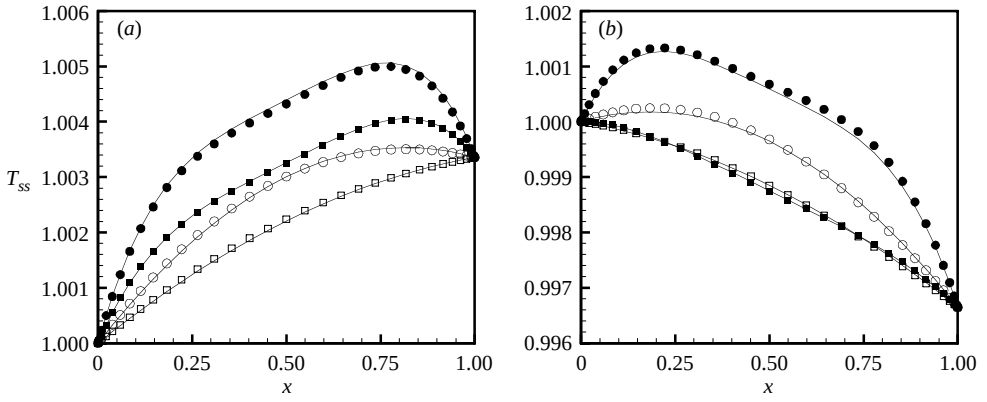

FIGURE 4. Comparison between narrow-gap solution and numerical solution for Dean (closed symbols) and Taylor–Couette (open symbols) flows. (*a*) $\Delta T^* = 1$ K (■, $Na = 0.061$; ●, $Na = 0.104$; □, $Na = 0.25$; ○, $Na = 0.1$). (*b*) $\Delta T^* = -1$ K (■, $Na = 0.016$; ●, $Na = 0.125$; □, $Na = 0.25$; ○, $Na = 0.1$). Symbols and lines represent numerical and analytical solutions respectively. $R_1/R_2 = 0.912$, $Pr = 7975.16$.

From a numerical fit, as shown in figure 4, one can approximate $g(x)$ as

$$g(x) = \begin{cases} A_1 x(1-x) & \text{(Taylor–Couette)}, \\ x(B_1 x^3 + B_2 x^2 + B_3 x + B_4) & \text{(Dean)}, \end{cases} \tag{21}$$

where the constants $A_1 \approx 0.5$ (Turian 1965; Bird, Armstrong & Hassaguer 1987), $B_1 \approx -10$, $B_2 \approx 19.9$, $B_3 \approx -15$ and $B_4 \approx 5.1$. Note that in the absence of an externally imposed temperature gradient, i.e. $\Delta T = 0$, equations (18)–(20) imply that the temperature rise due to viscous heating is $O(T^*/\varepsilon)$, consistent with the analysis of Pearson (1978).

3.2. *Linear stability analysis*

In this subsection, numerical results from a linear stability analysis are presented by using the numerically obtained steady-state profiles. As a model fluid we choose glycerin, as used in previous theoretical (Al-Mubaiyedh *et al.* 2002) and experimental (White & Muller 2000, 2002*a*, *b*) studies. For $T_0^* = 298.15$ K, the values of viscosity, density, specific heat capacity C_p and thermal conductivity k are 0.94 Pa s, 1261 kg m^{-3}, 2418 J kg^{-1} K^{-1} and 0.285 W m^{-1} K^{-1} respectively. Further, $\varepsilon = 24.88$ and Pr (at T_0^*) = 7975.16. We primarily use the gap ratio (R_1/R_2) of 0.912 used in previous Taylor–Couette experiments (White & Muller 2002*a*, *b*) although the influence of gap width is examined. Analysis is limited to a maximum ΔT^* of 1.5 K to minimize buoyancy effects.

In order to quantify the effect of viscous heating on the stability characteristics we use the parameter Λ defined as the ratio of the critical Reynolds number of the non-isothermal flow to that of the isothermal one. Plots of Λ vs. Na for Dean flow are shown in figure 5(*a*) for $\Delta T^* = 0$ and 1 K and for $0 \leqslant \xi \leqslant 2$. The most dangerous mode of disturbance is observed to be axisymmetric ($\xi = 0$) and stationary ($\sigma_I = 0$). An order-of-magnitude reduction in the critical Reynolds number is predicted for $O(1)$ values of Na, e.g. for $\Delta T^* = 0$, $\Lambda \approx 0.094$ for $Na = 0.2$. As expected, as $Na \to 0$, the critical conditions approach the isothermal limit ($\xi = 0$, $\alpha_c = 4.0$, $Re_c(d/R_1)^{1/2} = 40.81$).

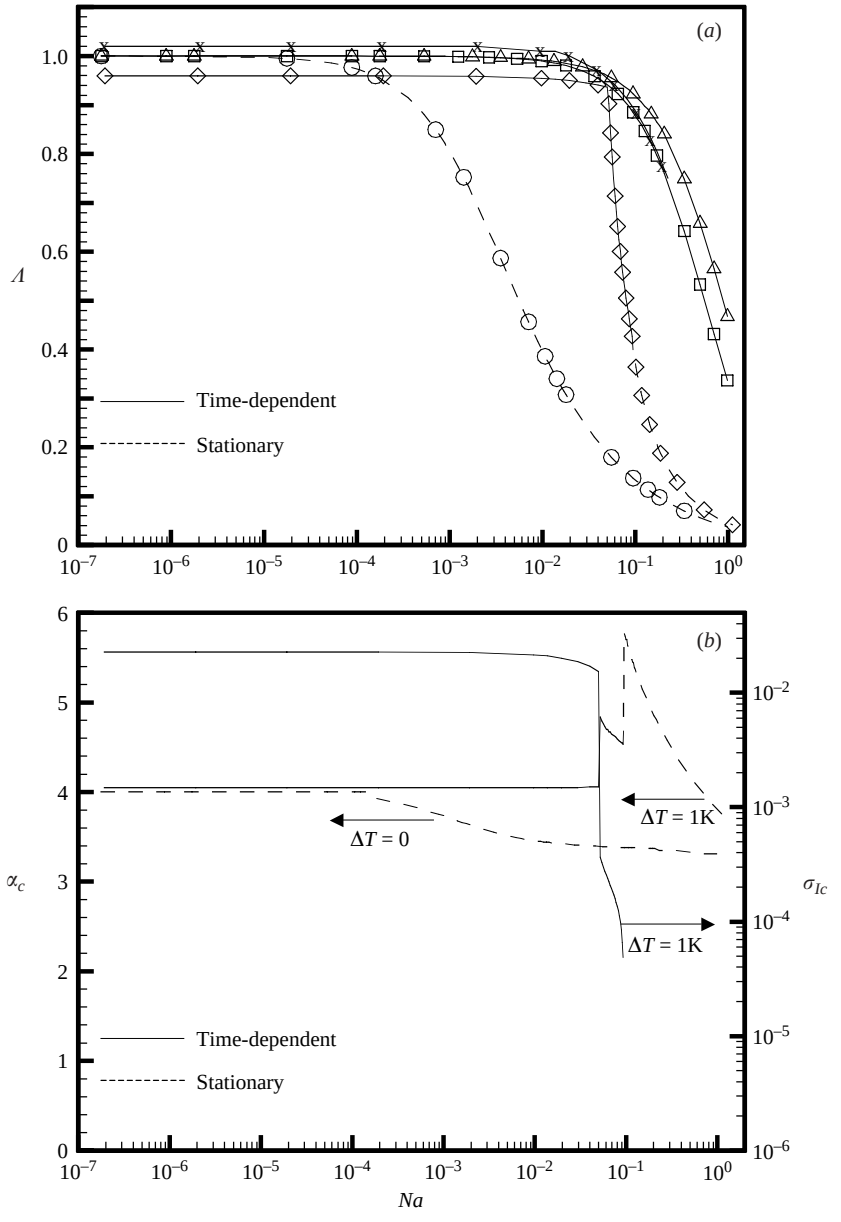

FIGURE 5. (*a*) Λ vs. *Na*. ○, $\xi = 0$, $\Delta T^* = 0$; ◇, $\xi = 0$, $\Delta T^* = 1\,\mathrm{K}$; □, $\xi = 1$, $\Delta T^* = 0$; ×, $\xi = 1$, $\Delta T^* = 1\,\mathrm{K}$; △, $\xi = 2$, $\Delta T^* = 0$. $R_1/R_2 = 0.912$, $Pr = 7975.16$ (Dean flow). (*b*) α_c vs. *Na* and σ_{Ic} vs. *Na*. $R_1/R_2 = 0.912$ (Dean flow).

The *Na* value for which the precipitous decrease in Re_c is initiated depends on the thermal boundary conditions. For $\Delta T^* = 0$, an appreciable reduction in Re_c can be seen even when *Na* is $O(10^{-2})$. This result is analogous to that reported by Al-Mubaiyedh *et al.* (2002) for Taylor–Couette flow where significant flow destabilization occurs for $O(10^{-2})$ values of *Na*. This is further explored in § 3.3. When $\Delta T^* = 1\,\mathrm{K}$, the most dangerous mode remains axisymmetric. However, the temporal characteristics

are time-dependent for $Na \leqslant 0.093$. For $Na \geqslant 0.093$ a stationary mode of instability is observed (figure 5*a*). Hence, thermal boundary conditions and Na influence the selection of the critical disturbance. In figure 5(*b*), the critical axial wavenumber, α_c, (for $\xi = 0$) is plotted for $\Delta T^* = 0$ and $\Delta T^* = 1\,\mathrm{K}$. For $\Delta T^* = 0$, α_c is practically constant at 4.0 for $Na < 0.0002$ and decreases to 3.31 for $O(1)$ Na. For $\Delta T^* = 1\,\mathrm{K}$, α_c remains nearly constant at 4.05 for $Na < 0.03$, and at $Na \approx 0.093$, there is a sharp increase in α_c to ≈ 5.8 when the change from a time-dependent to *a* stationary eigensolution occurs as shown in figure 5(*a*). The critical frequency, σ_{Ic}, corresponding to the time-dependent instability predicted for $\Delta T^* = 1\,\mathrm{K}$ is also plotted in figure 5(*b*). The temporal period associated with the eigenfunctions, $2\pi/\sigma_{Ic}$, can be found to be relatively large ($O(10^2)$–$O(10^5)$) with respect to the time scale d/V. However, the time period is more comparable to the thermal time scale (d^2/α_t) where α_t is the thermal diffusivity defined as $k/\rho C_p$. For instance, for $Na = 0.084$, the ratio of the time period of the oscillatory flow to the thermal time scale is 0.11.

The results reported in figures 5(*a*) and 5(*b*) are qualitatively similar to those obtained for Taylor–Couette flow (denoted by T–C) as shown in figures 6(*a*) and 6(*b*). However, the critical axial wavenumbers in Dean flow are larger than those in Taylor–Couette flow. Note that the results for Taylor–Couette flow are in agreement with those reported by Al-Mubaiyedh *et al.* (2002).

In figure 7, Re_c is plotted as a function of Na for two gap ratios, 0.85 and 0.95, for the axisymmetric mode of disturbance for three different gap temperature differences, 0, 1 K, 1.5 K. For a given gap width, the stationary mode corresponding to $\Delta T^* = 0$ becomes the most dangerous one for Nahme number greater than $O(10^{-4})$. As the temperature difference between the outer and inner cylinders is raised from 0 to 1.5 K, the critical mode changes from time-dependent to stationary for values of $Na > 0.1$. As in the case of isothermal flows the critical Reynolds number decreases with increasing gap width.

Snapshots of the secondary flow structures for the Dean and Taylor–Couette flows are presented in figures 8 and 9 respectively for different cases. Note that the radial velocity eigenfunctions are normalized with respect to the maximum value. The cellular structures corresponding to the critical eigenvalue for $\Delta T^* = 0$ are similar to those observed in the isothermal case. Oscillatory solutions observed for $\Delta T > 0$ for Dean flow show more complicated structure with localization near the outer wall.

3.3. *Scaling principles and mechanism of thermo-mechanical instability*

We now focus on the mechanism of the coupling between the energy and momentum equations that is responsible for the thermo-mechanical instability. Toward this end, a simplified linear stability model is developed for the stationary mode of instability for $Br \ll 1$ valid in the narrow-gap limit. Based on this model, a scaling law that relates Re_c, Na_c and Pr is developed to interpret the numerical results.

In order to guide the development of the simplified model we compute the onset conditions after turning off/on various terms in the linearized equations of motion and energy, which are given below for an axisymmetric mode of disturbance:

$$\frac{\partial \hat{T}}{\partial t} = -\underbrace{\hat{\boldsymbol{u}} \cdot \nabla T_{ss}}_{\mathrm{I}} + \frac{1}{Pe}\nabla^2 \hat{T} + \underbrace{\frac{Br}{2Pe} \mathrm{e}^{\varepsilon(1/T_{ss}-1)} \left(\boldsymbol{\kappa}_{ss} : \nabla \hat{\boldsymbol{u}} + \hat{\boldsymbol{\kappa}} : \nabla \boldsymbol{u}_{ss} - \frac{\varepsilon}{T_{ss}^2} \boldsymbol{\kappa}_{ss} : \nabla \boldsymbol{u}_{ss} \hat{T} \right)}_{\mathrm{II}}, \quad (22)$$

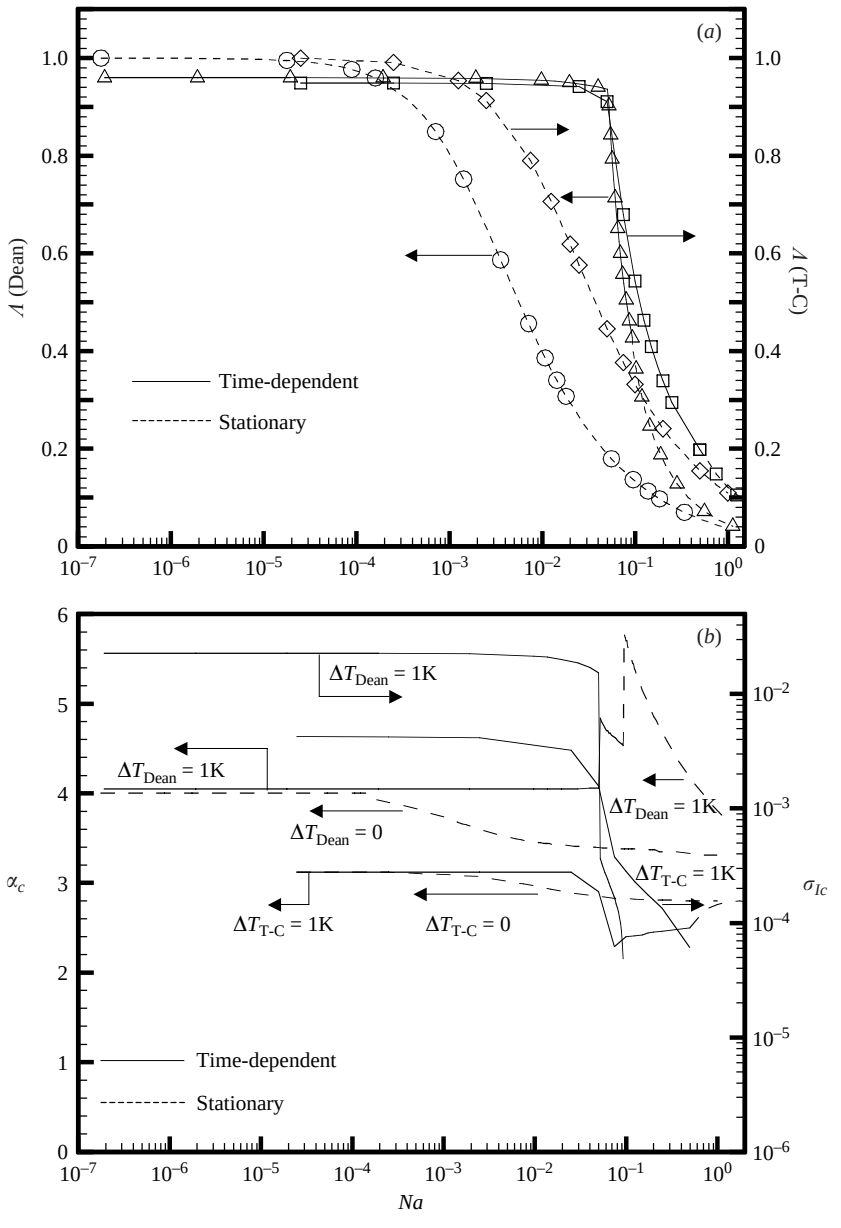

FIGURE 6. (*a*) Λ vs. *Na*. ○, ◇, $\xi = 0$, $\Delta T^* = 0$; △, □, $\xi = 0$, $\Delta T^* = 1\text{K}$. $R_1/R_2 = 0.912$. (*b*) α_c vs. *Na* and σ_{Ic} vs. *Na*. $R_1/R_2 = 0.912$ (Dean and Taylor–Couette (T–C) flows).

$$Re\left[\frac{\partial \hat{\boldsymbol{u}}}{\partial t} + \hat{\boldsymbol{u}}\cdot\nabla\boldsymbol{u}_{ss} + \boldsymbol{u}_{ss}\cdot\nabla\hat{\boldsymbol{u}}\right] = -Re\,\nabla P + \mathrm{e}^{\varepsilon(1/T_{ss}-1)}\left[\nabla^2\hat{\boldsymbol{u}} - \underbrace{\frac{\varepsilon}{T_{ss}^2}\nabla^2\boldsymbol{u}_{ss}\hat{T}}_{\text{III}}\right]$$

$$-\frac{\varepsilon}{T_{ss}^2}\mathrm{e}^{\varepsilon(1/T_{ss}-1)}\left[\underbrace{\boldsymbol{\kappa}_{ss}\cdot\nabla\hat{T}}_{\text{IV}} + \underbrace{\nabla T_{ss}\cdot\hat{\boldsymbol{\kappa}}}_{\text{V}} - \underbrace{\left(\varepsilon/T_{ss}^2 + 2/T_{ss}\right)(\nabla T_{ss}\cdot\boldsymbol{\kappa}_{ss})\hat{T}}_{\text{VI}}\right], \quad (23)$$

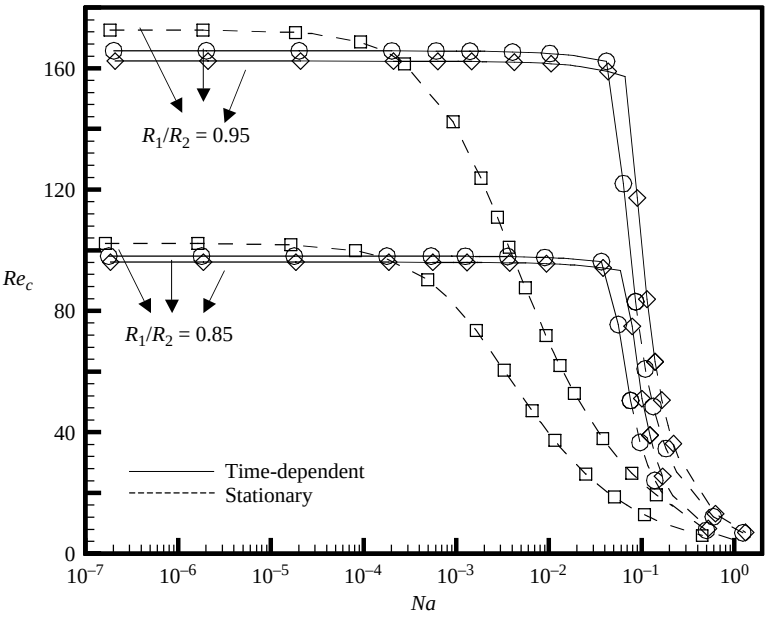

FIGURE 7. Influence of gap width and temperature difference (Dean flow). Re_c vs. Na ($\xi = 0$). □, $\Delta T^* = 0$; ○, $\Delta T^* = 1\text{K}$; ◇, $\Delta T^* = 1.5\,\text{K}$.

Terms turned off	Re_c	α_c
All terms due to thermal effects	131.36	4.0
None (non-isothermal)	50.72	3.45
I	130.43	4.0
II	50.72	3.45
III	69.35	2.44
IV	51.04	3.35
III, IV	129.43	4.0
IV, V, VI	50.95	3.45

TABLE 1. Influence of the various terms on the critical conditions.

where the hat symbol refers to the perturbation variables. The expanded forms of equations (22), (23) are given in Appendix B. A summary of the critical conditions obtained from the above procedure is tabulated in table 1. All the calculations reported are for $Na \approx 0.01$ for $\Delta T^* = 0$ and $\xi = 0\,(R_1/R_2 = 0.912)$. From the table, it is clear that terms I ($\hat{\boldsymbol{u}} \cdot \nabla T_{ss}$), III ($\varepsilon/T_{ss}^2 \nabla^2 \boldsymbol{u}_{ss} \hat{T}$) and IV ($\boldsymbol{\kappa}_{ss} \cdot \nabla \hat{T}$) greatly influence the predictions of the critical conditions since turning these terms off result in predictions that are close to the isothermal case ($Re_c = 131.36$, $\alpha_c = 4.0$). Hence, the underlying mechanism driving the destabilization results from the coupling of the perturbation radial velocity and the base-state temperature gradient, i.e. the term $\hat{\boldsymbol{u}} \cdot \nabla T_{ss}\,(= \hat{\boldsymbol{u}}_r \cdot \mathrm{d}T_{ss}/\mathrm{d}r)$ appearing in the energy equation. It is evident from the discussion in § 3.1 that $u_{\theta ss} \approx u_{\theta ss,iso}$, i.e. the angular momentum distribution is practically unchanged. However, as pointed out by Al-Mubaiyedh *et al.* (2002), the temperature enhancement reduces the local viscosity and lowers the ability of the fluid to dampen velocity perturbations. This is further demonstrated by the observation that for negative values of ΔT^*, destabilization is very pronounced even in the absence of

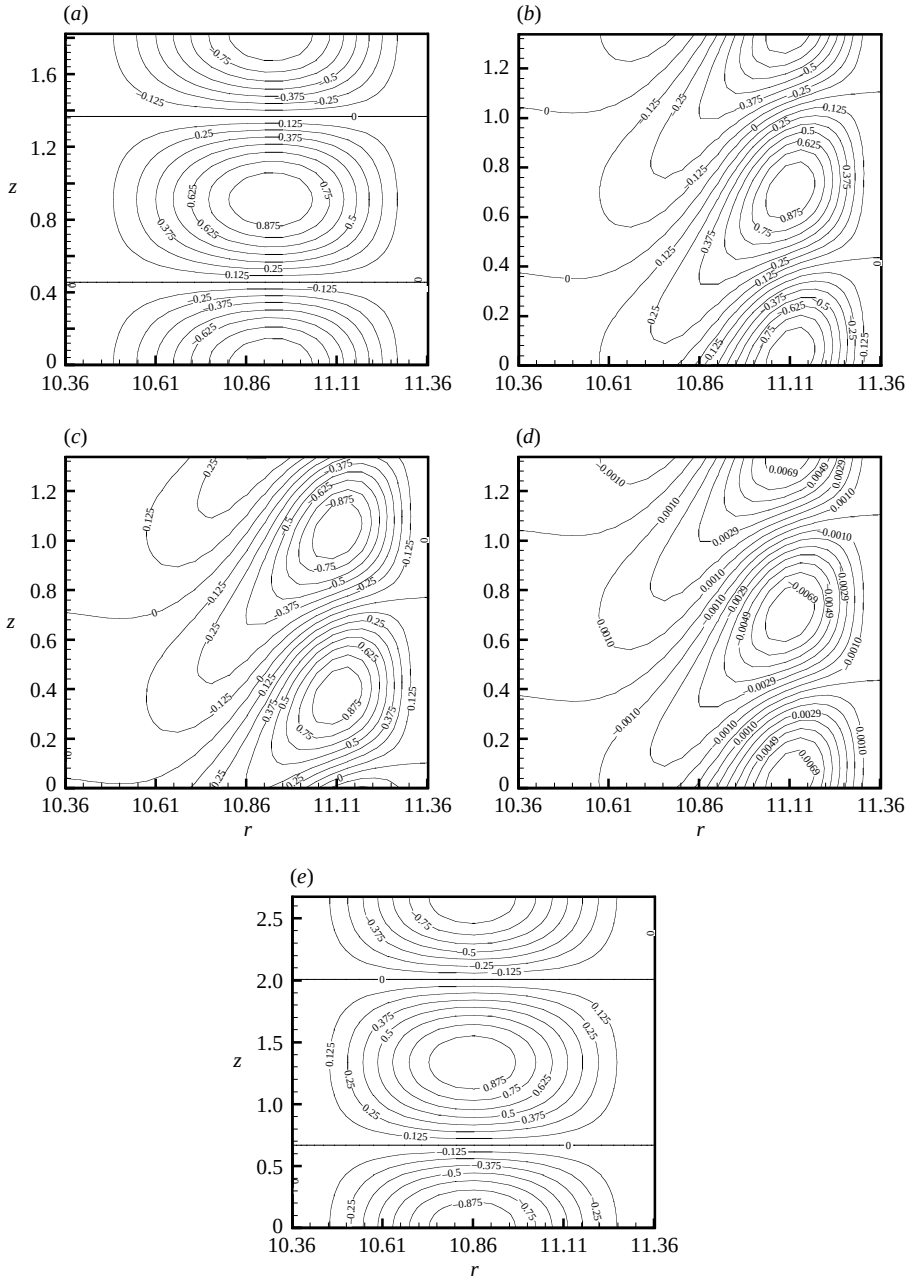

FIGURE 8. Radial velocity contour plots at critical conditions for Dean flow at $\Delta T^* = 0$ ($Na = 0.01$, $Re_c = 50.72$, $\alpha_c = 3.45$ (stationary)), $\Delta T^* = 1\text{K}$ ($Na = 0.06$, $Re_c = 93.78$, $\alpha_c = 4.7$ (time-dependent)) and $\Delta T^* = -1\text{K}$ ($Na = 0.09$, $Re_c = 5.73$, $\alpha_c = 2.35$ (stationary)) (*a*) $\Delta T^* = 0$. (*b*) $\Delta T^* = 1\text{K}$ ($t = 0$). (*c*) $\Delta T^* = 1\text{K}$ ($t = (2\pi/\sigma_I)/4$). (*d*) $\Delta T^* = 1\text{K}$ ($t = (2\pi/\sigma_I)/2$). (*e*) $\Delta T^* = -1\text{K}$.

viscous heating ($Br = 0$) as shown in figure 10. Specifically, when $\Delta T < 0$, the largest reduction in viscosity occurs near the inner cylinder. Hence the radial velocity perturbations in this region encounter relatively lower dissipative forces.It can also be seen

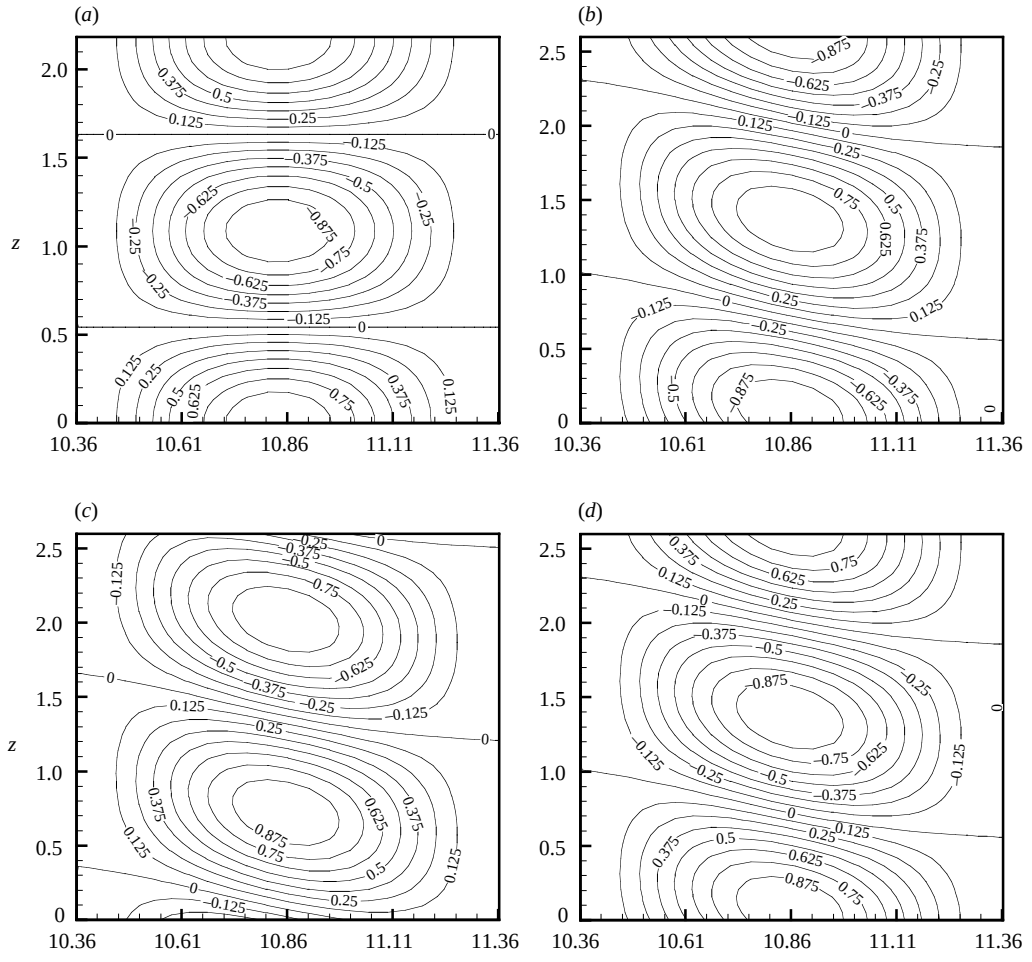

FIGURE 9*a–d*. For caption see facing page.

from figure 10 that in the limit as $Br \to 0$, positive values of ΔT have only a very mild destabilizing effect on the flow. However, the most dangerous disturbance is time-dependent for $\Delta T > 0$. As shown in figures 5(*a*) and 6(*a*), this mode of disturbance is severely destabilizing in the presence of viscous heating.

A simplified quantitative model of the proposed mechanism can be developed: see Appendix C for the derivation. Specifically, the coupling between the radial perturbation velocity and the base-state temperature gradient causes an amplification of the temperature perturbation ($\hat{T}$) according to the following relationship obtained by re-arranging equation (C 13):

$$\hat{T} = -\frac{Pe}{\alpha^2}\frac{\mathrm{d}T^{ss}}{\mathrm{d}r}\hat{u}_r. \tag{24}$$

Equation (24) implies that the convection of base-state temperature gradient by radial velocity perturbations results in enhanced thermal fluctuation within the flow since Pe/α^2 is $\gg 1$ for high-Pr liquids. Substituting for $\hat{T}$ and $\hat{u}_r$, and using normal-mode

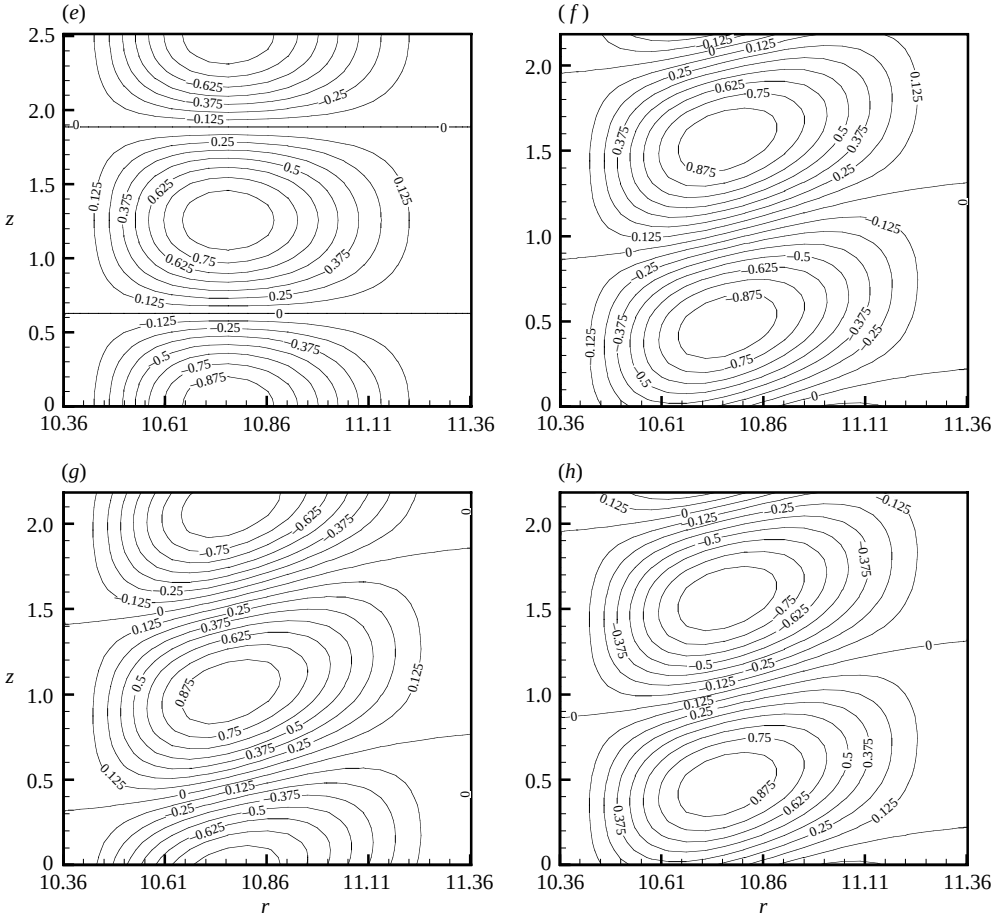

FIGURE 9. Radial velocity contour plots at critical conditions for Taylor–Couette flow at $\Delta T^* = 0$ ($Na = 0.025$, $Re_c = 80.62$, $\alpha_c = 2.89$ (stationary)), $\Delta T^* = 1\text{K}$ ($Na = 0.1$, $Re_c = 76.08$, $\alpha_c = 2.42$(time-dependent)) and $\Delta T^* = -1\text{K}$ ($Na = 0.25$, $Re_c = 27.88$, $\alpha_c = 2.5$ (stationary); $Na = 0.1$, $Re_c = 47.15$, $\alpha_c = 2.88$ (time-dependent)) (*a*) $\Delta T^* = 0$. (*b*) $\Delta T^* = 1\text{K}$ ($t = 0$). (*c*) $\Delta T^* = 1\text{K}$ ($t = (2\pi/\sigma_I)/4$). (*d*) $\Delta T^* = 1\text{K}$ ($t = (2\pi/\sigma_I)/2$). (*e*) $\Delta T^* = -1\text{K}$ (stationary). (*f*) $\Delta T^* = -1\text{K}$ ($t = 0$). (*g*) $\Delta T^* = -1\text{K}$ ($t = (2\pi/\sigma_I)/4$). (*h*) $\Delta T^* = -1\text{K}$ ($t = (2\pi/\sigma_I)/2$).

expansions, one obtains

$$\left(\hat{T}_R + \frac{Pe}{\alpha^2}\frac{\mathrm{d}T_{ss}}{\mathrm{d}r}\hat{u}_{r,R}\right)\cos(\alpha z) - \left(\hat{T}_I + \frac{Pe}{\alpha^2}\frac{\mathrm{d}T_{ss}}{\mathrm{d}r}\hat{u}_{r,I}\right)\sin(\alpha z) = 0, \tag{24a}$$

where subscripts 'R' and 'I' denote the real and imaginary parts of the corresponding eigenfunction respectively. Multiplying equation (24*a*) by $r\cos(\alpha z)(r\sin(\alpha z))$ and integrating in the domain ($r_1 \leqslant r \leqslant r_2$, $0 \leqslant z \leqslant 2\pi/\alpha$) gives

$$\int_{r_1}^{r_2}\left(\hat{T}_{R(I)} + \frac{Pe}{\alpha^2}\frac{\mathrm{d}T_{ss}}{\mathrm{d}r}\hat{u}_{r,R(I)}\right) r\,\mathrm{d}r = 0. \tag{24b}$$

The above assertion is verified by using results obtained from the numerical linear

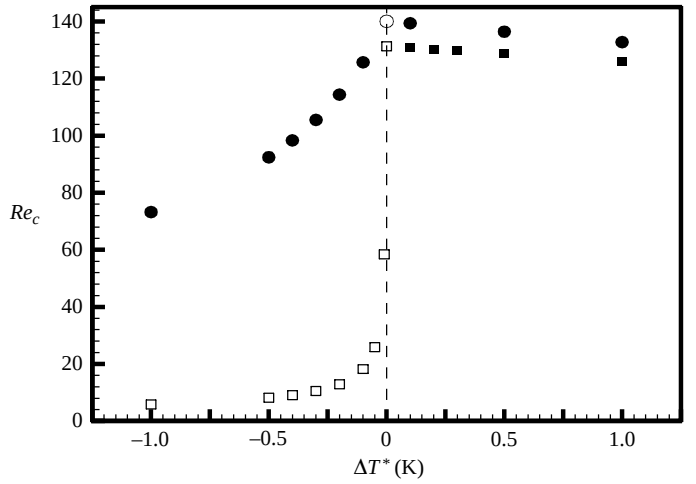

FIGURE 10. Re_c vs. ΔT^* at $Br = 0$ for Dean (■, □) and Taylor–Couette (●, ○) flows. Open and closed symbols correspond to stationary and time-dependent modes respectively.

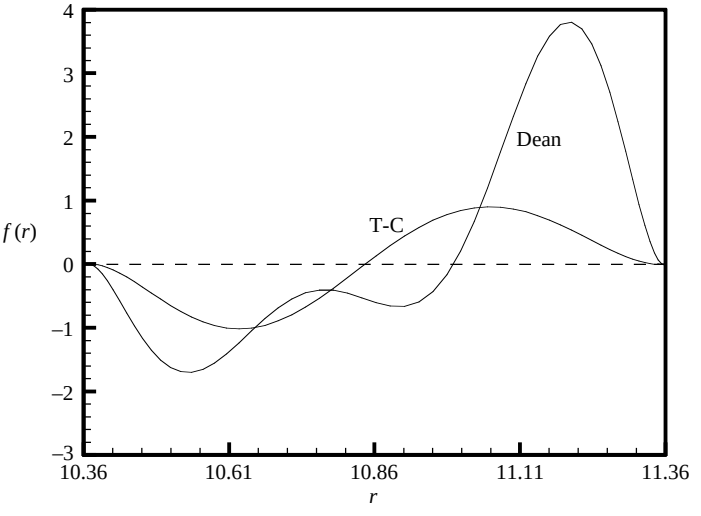

FIGURE 11. $f(r)$ vs. r at $\Delta T^* = 0$ for Taylor–Couette flow ($Na = 0.1$, $Re_c = 46.43$, $\alpha_c = 2.83$) and Dean flow ($Na = 0.01$, $Re_c = 50.72$, $\alpha_c = 3.45$).

stability analysis. As shown in figure 11, the integrand

$$f(r) \equiv \hat{T}_R + \frac{Pe}{\alpha^2}\frac{\mathrm{d}T_{ss}}{\mathrm{d}r}\hat{u}_{r,R}$$

is approximately antisymmetric with respect to the mid-plane of the gap for the Taylor–Couette flow. Although the analogous curve corresponding to Dean flow is not antisymmetric, it passes through both negative and positive values such that the area under the curve remains small. Numerical integration shows that

$$\int_{r_1}^{r_2} rf(r)\,\mathrm{d}r \ll \sqrt{\int_{r_1}^{r_2} rf^2(r)\,\mathrm{d}r}.$$

Hence, the above mechanism is equally valid for both Taylor–Couette and Dean flows. Further, as shown in Appendix C, equation (24) can be combined with the linearized momentum equation to obtain a master equation valid for both Taylor–Couette and Dean flows:

$$\frac{\mathrm{d}^2\hat{u}_r}{\mathrm{d}r^2} + \left[\alpha^2 + \frac{2ReUU'}{\alpha^2 r}\right]\hat{u}_r = \frac{2ReUK\Theta'}{\alpha^2 r}\left[U'\frac{\mathrm{d}\hat{u}_r}{\mathrm{d}r} + U''\hat{u}_r\right]$$

(equation (C 13)), where $K \equiv \varepsilon Pe/(T_{ss}\alpha)^2$, $\Theta' \equiv \mathrm{d}T_{ss}/\mathrm{d}r$, $U \equiv u_{\theta ss}$, $U' \equiv u'_{\theta ss}$ and $U'' \equiv u''_{\theta ss}$.

Use of equation (16), $\Theta' = S + cNa$ and $S = \varepsilon\Delta T$ in (C 13) results in the following scaling law for $\Delta T = 0$ (see the Appendix for derivations leading to equations (C 13), (C 24) and (C 31)):

$$\Lambda = \frac{1}{\left[1 - PrcNa/\left(T_{ss}^2\alpha^2\right)\right]^{1/2}}, \tag{25}$$

where $c < 0$ is a flow-dependent constant that can be determined by fitting the numerical results obtained for Λ to equation (25). Equation (25) can be written in the following form:

$$\left(\frac{1}{\Lambda^2} - 1\right)\frac{\alpha^2}{Pr} = -\frac{cNa}{T_{ss}^2}. \tag{26}$$

From a numerical fit of equation (26) shown in figure 12 to a linear equation of the form $y = a\,x$, where

$$y = \left(\frac{1}{\Lambda^2} - 1\right)\frac{\alpha^2}{Pr}, \quad x = Na, \quad a \equiv -\frac{c}{T_{ss}^2}, \tag{27}$$

we obtain $a = 0.08$ and 0.8 for Taylor–Couette and Dean flows respectively.

In general, as discussed in § 3.2, for non-zero values of ΔT the most dangerous eigenvalue is time-dependent. For Taylor–Couette flow with non-zero ΔT, the scaling law can be written as

$$\Lambda = \begin{cases} \dfrac{1}{\left[1 - \left(Pr/T_{ss}^2\alpha^2\right)(S + c_1 Na)\right]^{1/2}} & \text{(Taylor–Couette flow)}, \\ \dfrac{1}{\left[1 - \left(c_3 Pr/T_{ss}^2\alpha^2\right)(S + c_2 Na)\right]^{1/2}} & \text{(Dean flow)} \end{cases}$$

(equations (C 24) and (C 31) in the Appendix). Equation (C 24) suggests that even in the absence of viscous heating ($Br \to 0$, i.e. $c_1 \equiv 0$), an externally imposed thermal gradient can be destabilizing if $\Delta T < 0$. Note that equation (A 36) is strictly valid for stationary disturbances. Nevertheless, as shown in figure 12(*c*) this scaling relationship applies even for the time-dependent mode of instability. Specifically $1/\Lambda^2$ scales linearly with ΔT for $\Delta T < 0$. This should not be surprising since for time-dependent eigensolutions, equation (C 1) is not qualitatively modified, i.e. at the critical point, $\sigma = 0$ and σ_I for stationary and time-dependent modes respectively. This only changes the numerical constants and does not qualitatively affect the mechanism of thermo-mechanical coupling. For Dean flow, the critical disturbance is stationary for $\Delta T < 0$ (see figure 10). Hence, as $Br \to 0$ ($c_2 = 0$), $1/\Lambda^2$ should scale linearly with ΔT if $c_3 < 0$. This is found to be the case as reported in figure 12(*c*).

In general, the scaling analysis suggests that for sufficiently large values of Na ($Na \gg \varepsilon\Delta T$ and $Pr\,cNa/(T_{ss}^2\alpha^2) \gg 1$), a power-law relationship of the form

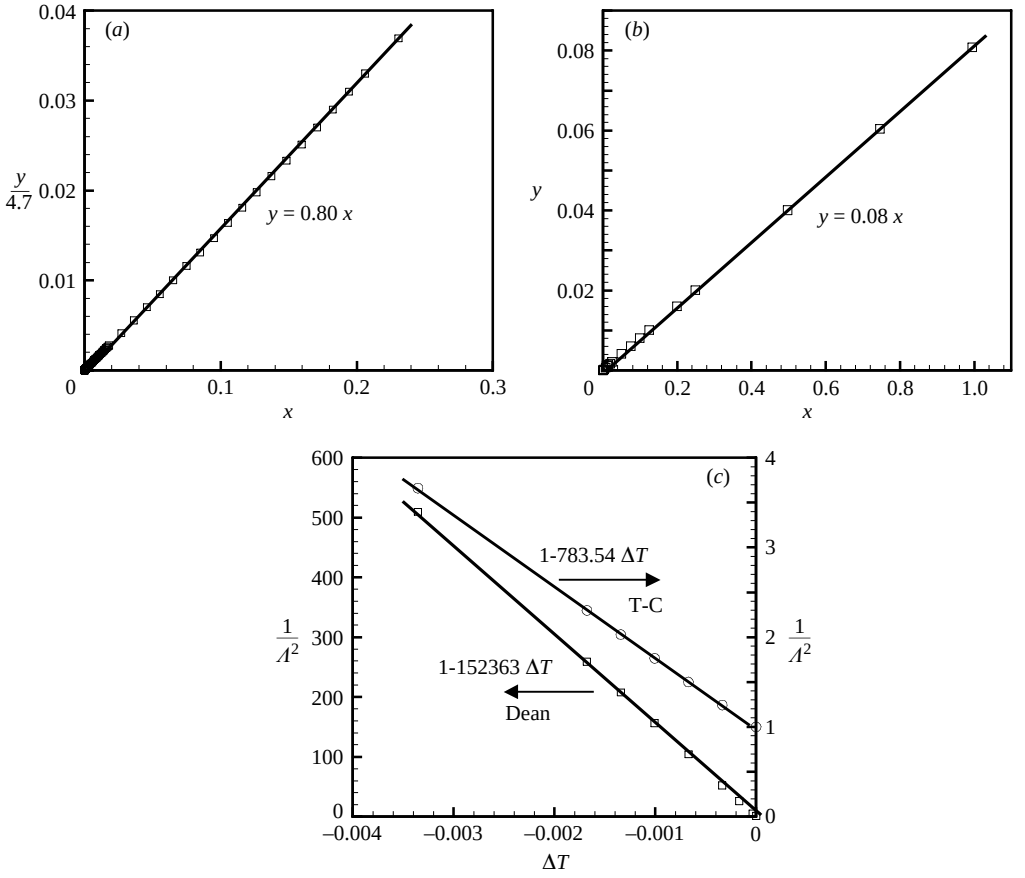

FIGURE 12. Scaling law for the critical conditions at $\Delta T^* = 0$: (*a*) Dean flow, (*b*) Taylor–Couette flow. $y = (1/A^2 - 1)\alpha^2/Pr$ and $x = Na$. (*c*) Scaling with ΔT for $Br = 0$.

ΔT^* (K)	p (Dean)	p (Taylor–Couette)
0	0.5	0.43
0.25	0.78	0.54
0.5	0.84	0.58
1.0	1.01	0.62
1.3	1.02	0.62
1.5	1.16	0.68

TABLE 2. Dependence of power law exponent (p) on ΔT^*.

$Re_c\sqrt{\delta} = K\,Na^{-p}$, $p > 0$, should exist irrespective of the temporal characteristics of the instability. Figure 13 shows a log-log plot of $Re_c(d/R_1)^{1/2}$ versus Na for the most dangerous (axisymmetric) disturbance. For $Na > 0.01$, a power-law relationship with $p = 1/2$ and 1 can be seen for $\Delta T^* = 0$ and $\Delta T^* = 1$ K, respectively. The value of the exponent p depends on the imposed temperature boundary conditions. This is evident also from table 2, where p is tabulated against ΔT^* in the range 0 to 1.5 K for Dean and Taylor–Couette flows.

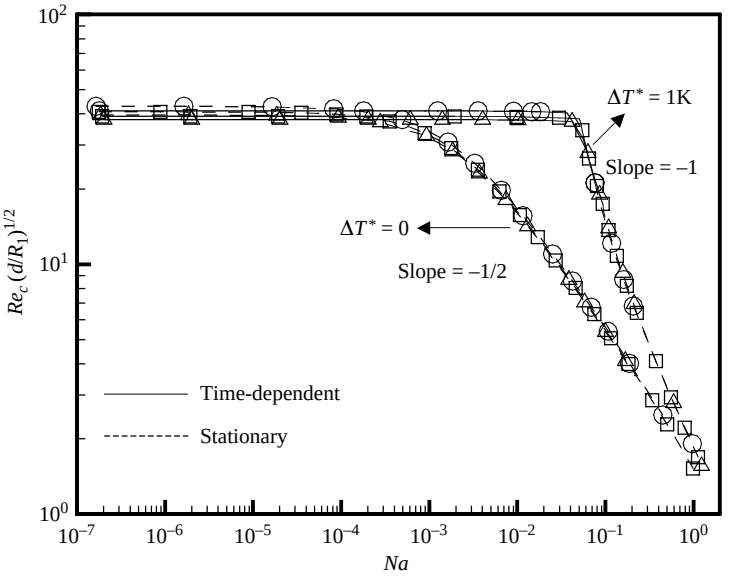

FIGURE 13. $Re_c(d/R_1)^{1/2}$ vs. Na (log-log plot). ○, $R_1/R_2 = 0.85$; □, $R_1/R_2 = 0.912$; △, $R_1/R_2 = 0.95$. $T_0^* = 298.15$ K (Dean flow).

3.4. *Nonlinear stability analysis*

In this subsection, we present results for the nonlinear evolution of the thermo-mechanical instability for Dean flow by performing time-dependent simulations. The initial condition is obtained by a superposition of the eigenfunctions associated with the most unstable eigenvalue and the steady-state solution. It is known that for Taylor–Couette flow (Al-Mubaiyedh *et al.* 2002) the bifurcation to the secondary time-dependent state is weakly subcritical, while that to the secondary stationary state is supercritical. However, in the case of Dean flow, the bifurcations to both the time-dependent and stationary secondary states are found to be supercritical.

The time-dependent simulations are performed by starting from an initial condition at a shear rate that is slightly greater than that at the bifurcation point. Two reference temperatures, $T_0^* = 318$ K and $T_0^* = 322$ K are chosen to investigate stationary and time-dependent modes respectively. Specifically, for $T_0^* = 318$ K and $\Delta T^* = 0$, the most unstable mode of disturbance is stationary with $\alpha_c = 3.42$, $\dot{\gamma}_c = 1873.2\,\mathrm{s}^{-1}$, $Re_c = 45.59$ and $Na_c = 0.06$, where $\dot{\gamma}_c$ is the shear rate corresponding to $Re_c = 45.59$ for glycerin and $R_1 = 6.946$ cm as in experiments (White & Muller 2002*a*, *b*). The growth of the radial velocity at $r = (r_1 + r_2)/2$ and $z = \pi$ is plotted against time in figure 14 for $\dot{\gamma} = 1905\,\mathrm{s}^{-1}$ ($Re - Re_c = 0.81$), which shows that the bifurcation results in a new stationary solution. The bifurcation diagram, i.e. the plot of amplitude vs. $Re - Re_c$, shows supercritical flow transition as shown in figure 15. The inset to figure 14 shows the contour plot of the radial velocity for the new state. For $T_0^* = 322$ K and $\Delta T^* = 1$ K, time-dependent modes are the most unstable with $\alpha_c = 4.57$, $\dot{\gamma}_c = 2683.15\,\mathrm{s}^{-1}$, $Re_c = 91.60$ and $Na_c = 0.1$. The bifurcation to the time-dependent state is also supercritical as shown in figure 16. The growth of the maximum radial velocity at $r = (r_1 + r_2)/2$ and $z = \pi$ is plotted against time in figure 16 (inset) for $\dot{\gamma} = 2700\,\mathrm{s}^{-1}$ ($Re - Re_c = 0.62$) showing that the flow evolves into a limit cycle. The radial velocity (normalized with respect to the maximum value) contours at points where $u_r|_{r=\frac{1}{2}(r_1+r_2),z=\pi}$ is minimum, zero and maximum are shown in figure 17. As in the case of the corresponding

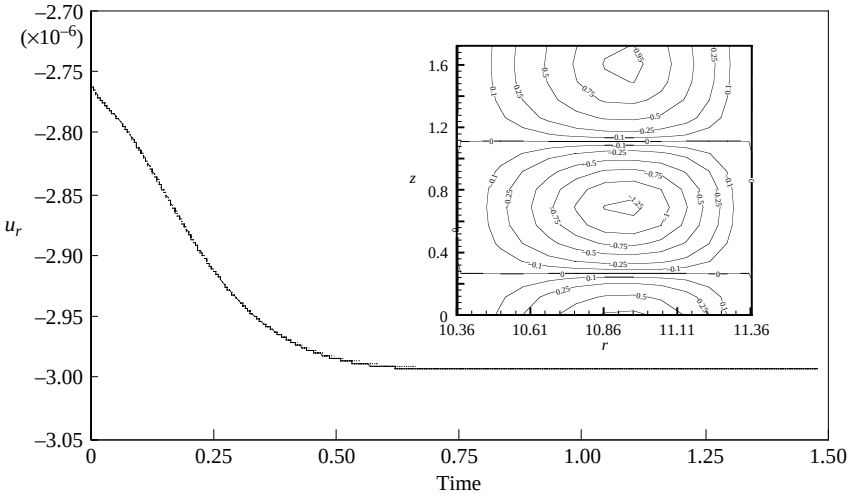

FIGURE 14. Time-dependent evolution of radial velocity at $(r = (r_1+r_2)/2$ and $z = \pi)$ for $T_0^* = 318$ K, $\Delta T^* = 0$, $\alpha = 3.42$, $\dot{\gamma} = 1905\,\mathrm{s}^{-1}$ and $Re{-}Re_c = 0.81$. The inset shows radial velocity contour plots.

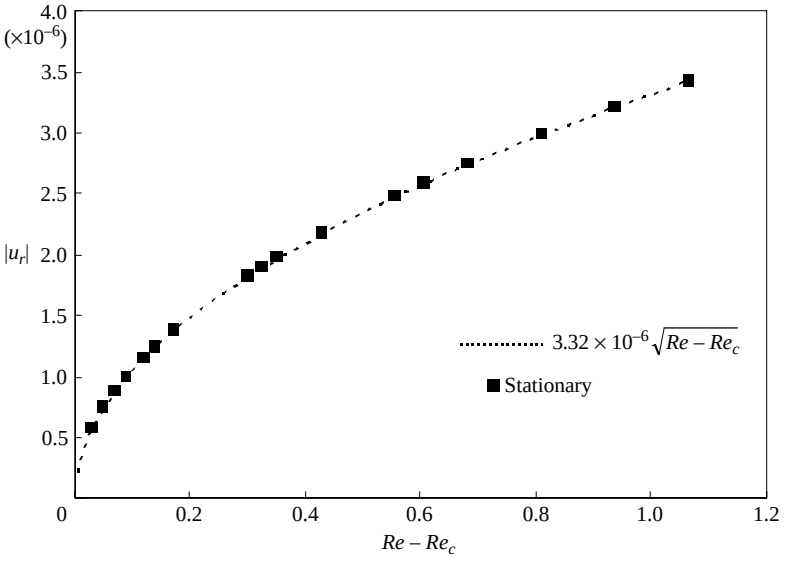

FIGURE 15. Bifurcation diagram for $T_0^* = 318$ K, $\Delta T^* = 0$ and $\alpha = 3.42$ $(Re_c = 45.59)$.

eigenfunctions for $T_2 > T_1$ (figure 8), the radial velocity attains its maximum value at a location closer to the outer cylinder. Finally, we note that the time axes in figures 14 and 16 are scaled with respect to the thermal diffusion time scale, d^2/α_t. It can be seen that the inception time, i.e. the transient period during which the finite-amplitude disturbances grow towards the secondary flow state, is comparable to d^2/α_t.

4. Conclusions

In this work, we have investigated the influence of thermal effects on centrifugal flow instabilities of Newtonian fluids whose viscosity is sensitive to temperature. In order to

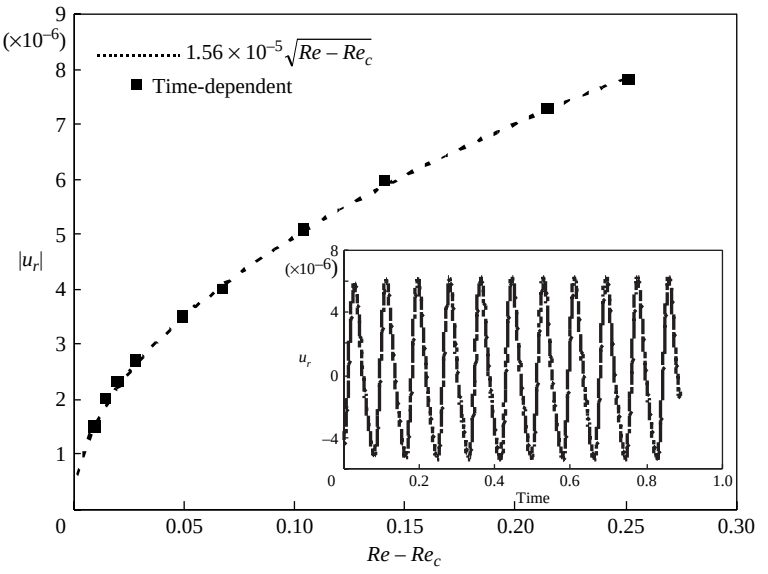

FIGURE 16. Bifurcation diagram for $T_0^* = 322$ K, $\Delta T^* = 1$ K and $\alpha = 4.57$ ($Re_c = 91.60$). The inset diagram shows the time-dependent evolution of radial velocity at ($r = (r_1 + r_2)/2$ and $z = \pi$) for $T_0^* = 322$ K, $\Delta T^* = 1$ K, $\alpha = 4.57, \dot{\gamma} = 2700\,\mathrm{s}^{-1}$ and $Re - Re_c = 0.62$.

ascertain the role of the driving force, i.e. pressure-driven vs. drag-driven flows, Dean and Taylor–Couette flows are considered. Even in the absence of viscous heating, thermal sensitivity effects could be important if a temperature difference is externally imposed across the gap. Hence we have focused on two limiting cases, namely the role of viscous heating when both cylinders are kept at the same temperature and that of an externally imposed thermal gradient in the absence of viscous heating. The synergistic effect of the two sources of thermal non-homogeneity is also considered. In addition to numerical linear stability analysis results for the onset conditions and the spatio-temporal characteristics of the most dangerous disturbance, a simplified model has been developed to explain the precise mechanism of thermo-mechanical coupling. This model, together with analytical results for the base-state temperature and velocity profiles, allow the derivation of scaling laws that relate the critical Reynolds and Nahme numbers, the Prandtl number of the fluid and a dimensionless parameter S which is the product of the activation energy associated with fluid viscosity and externally imposed temperature difference.

In all cases considered, the maximum temperature difference within the gap is small enough so that the base-state velocity profile and the distribution of angular momentum remain practically unchanged from those in the isothermal flow. Hence, the base-state temperature gradient is approximated as a linear superposition of the contribution from the temperature difference imposed externally and that from viscous heating. The maximum temperature difference considered is less than 2 K. Even under such conditions, both Dean and Taylor–Couette flows are greatly destabilized, i.e. the onset of centrifugal instability occurs at Reynolds number values lower than that of the isothermal flow, even for Nahme number values as small as $O(10^{-3})$. This is due to the thermo-mechanical coupling resulting from the convection of the base-state thermal gradient by radial velocity perturbations leading to enhanced temperature fluctuations. Specifically, it has been shown that the ratio of the magnitudes of

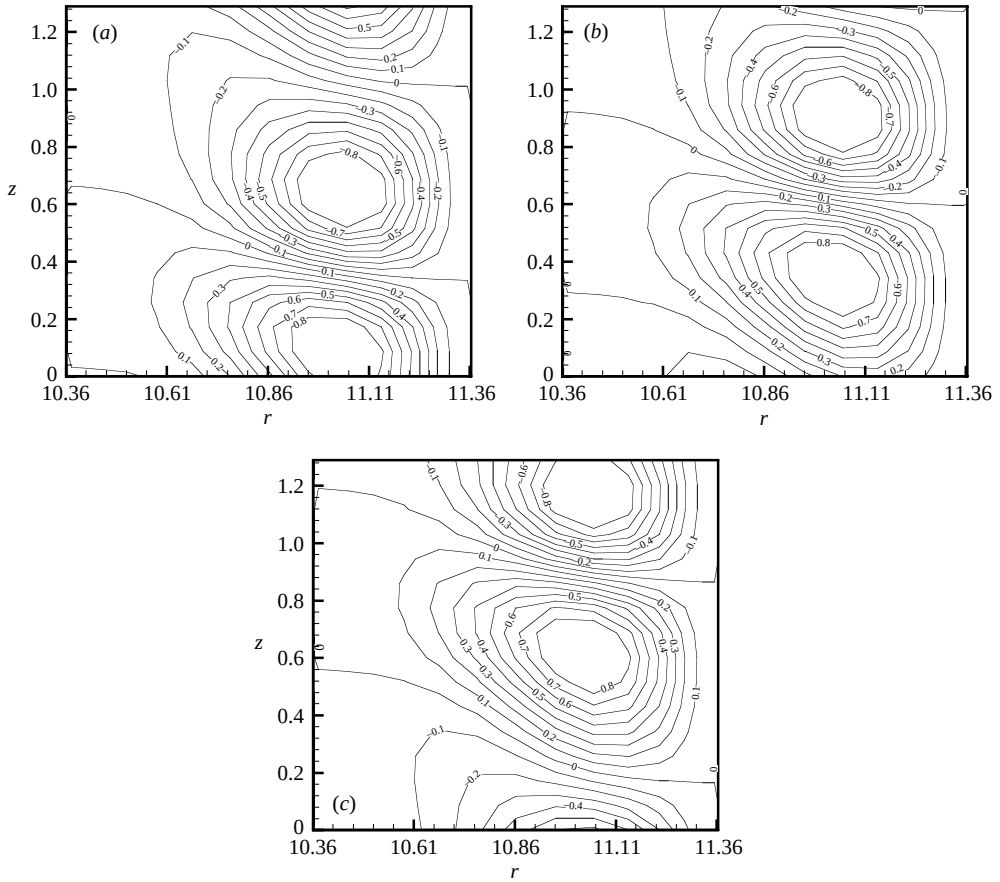

FIGURE 17. Radial velocity contours for the final state in figure 8 for $T_0{}^* = 322$ K, $\Delta T^* = 1$ K, $\alpha = 4.57$, $\dot{\gamma} = 2700\,\mathrm{s}^{-1}$ and $Re{-}Re_c = 0.62$ where amplitude is (*a*) minimum, (*b*) zero and (*c*) maximum.

thermal and radial velocity perturbations is proportional to Pe/α^2 where Pe is the Péclet number and α is the dimensionless axial wavenumber of the critical disturbance. For high-Prandtl-number liquids, this ratio is $\gg 1$. Consequently, in the absence of external thermal gradients, the precipitous decrease in the critical Reynolds number occurs when Na is $O(\alpha^2/Pr)$. Since α^2 is $O(10)$ and Pr could be $O(10^4)$ for highly thermally sensitive fluids like glycerin, this means that $O(10^{-3})$ values of Na are sufficient to cause significant flow destabilization. A scaling law of the form $\Lambda = [1 + Prc_1 Na/\alpha^2]^{-1/2}$, where c_1 is a flow-dependent constant, is derived to quantify the thermo-mechanical effect caused by viscous heating when $\Delta T = 0$ where Λ denotes the ratio of the critical Reynolds numbers for the non-isothermal and isothermal flows.

In the absence of viscous heating, it has been found that negative values of ΔT have a deleterious effect on flow stability. For instance, an order-of-magnitude reduction in Re_c is predicted when the temperature of the inner cylinder is maintained at 1°C above that of the outer one for Dean flow. Note that when $\Delta T < 0$, the largest reduction in viscosity occurs near the inner cylinder. Hence the radial velocity perturbations in this region encounter relatively lower viscous dissipation. It has been shown that when

$\Delta T < 0$ and in the limit as $Br \to 0$, $\Lambda = [1 + Pr\, c_2 S/\alpha^2]^{-1/2}$, where $c_2 < 0$ is a flow-dependent constant and $S \equiv \varepsilon \Delta T$. This indicates that a significant reduction in Re_c will occur when $S\, Pr/\alpha^2 \gg 1$, consistent with the result of the numerical linear stability analysis. In the limit as $Br \to 0$ with $\Delta T > 0$, the influence of the external thermal gradient on Re_c is negligible. However, the critical disturbance is time-dependent and axisymmetric compared to stationary toroidal vortex structures predicted for $\Delta T = 0$. However, viscous heating and positive values of ΔT still cause flow destabilization. When $\Delta T > 0$ and viscous heating is present, numerical linear stability analysis shows that $\Lambda \propto Na^k$ where $k < 0$ is dependent on the flow and ΔT.

A nonlinear stability analysis of Dean flow indicates that the bifurcation is supercritical for both stationary ($\Delta T = 0$) and time-dependent ($\Delta T > 0$) modes of instabilities. In comparison, in the Taylor–Couette flow, the nonlinear evolution of the time-dependent disturbance is weakly subcritical while the stationary instability is supercritical (Al-Mubaiyedh *et al.* 2002).

The authors gratefully acknowledge the financial support of this research from NSF through Grants CTS-9874813 and CTS-0132730.

Appendix A. Constants in the perturbation base-state solution

The constants in equations (8)–(11) for Dean flow are given by

$$C_1 = \frac{\ln(1+\delta)(1+\delta)^2}{\delta^4(\delta+2)}, \quad C_2 = \frac{\ln(1+\delta)(1+\delta)^2}{2\delta^2(\delta+2)} - \frac{\ln\delta}{2\delta}, \tag{A 1}$$

$$C_3 = \frac{1}{\ln(1+\delta)}\left[\frac{-C_1^2\delta^3(\delta+2)}{4(1+\delta)^2} + \frac{(\delta+2)}{16\delta^3} + \frac{C_1\ln(1+\delta)(2\ln\delta - \ln(1+\delta))}{2\delta}\right], \tag{A 2}$$

$$C_4 = C_3\ln\delta - C_1\frac{(\ln\delta)^2}{2\delta} + \frac{C_1^2\delta^2}{4} + \frac{1}{16\delta^4}, \tag{A 3}$$

$$\begin{aligned} C_5 = {} & -\frac{C_1(C_3+2C_4)}{2} + \frac{2(1+\delta)^2}{\delta^3(\delta+2)} \\ & \times\left[\frac{C_1^3\delta^4}{16}\left(1 - \frac{1}{(1+\delta)^4}\right) - \frac{(\delta+2)}{64\delta^4} + \frac{C_1C_3\delta^2}{2}\left\{\frac{\ln((1+\delta)/\delta)}{(1+\delta)^2} + \ln\delta\right\}\right. \\ & + \frac{C_1^2\delta}{16}\left\{\frac{3}{(1+\delta)^2} - 3 + \frac{4\ln((1+\delta)/\delta)}{(1+\delta)^2} + 4\ln\delta + \frac{4(\ln((1+\delta)/\delta))^2}{(1+\delta)^2} - 4(\ln\delta)^2\right\} \\ & + \frac{C_1(3\ln(1+\delta) + 4(\ln((1+\delta)/\delta))^3 + 4(\ln\delta)^3)}{48\delta^2} \\ & \left. + \frac{(2C_4\ln(1+\delta) + C_3(\ln((1+\delta)/\delta))^2 - C_3(\ln\delta)^2)}{4\delta}\right], \end{aligned} \tag{A 4}$$

and

$$\begin{aligned} C_6 = {} & -\frac{C_1^3\delta^4}{16} - \frac{1}{64\delta^5} + \frac{(C_1C_3 + 2C_1C_4 - 2C_1C_3\ln\delta + 2C_5)\delta^2}{4} \\ & - \frac{C_1\ln\delta(3 + 4(\ln\delta)^2)}{48\delta^2} - \frac{\ln\delta(2C_4 - C_3\ln\delta)}{4\delta} + \frac{(3 - 4\ln\delta + 4(\ln\delta)^2)C_1^2\delta}{16}. \end{aligned} \tag{A 5}$$

The constants in equation (13) for Taylor–Couette flow are given by

$$A = \frac{(\zeta^2+5)(\zeta^2-1) - 2\zeta^2 \ln\zeta - 8\ln\zeta)}{4(\zeta^2-1)^3 \ln\zeta}, \tag{A 6}$$

and

$$B = \frac{-1}{2(\zeta^2-1)^3} - \left(\frac{2}{(\zeta^2-1)^2} - 2A\ln\zeta - \frac{4\ln\zeta}{(\zeta^2-1)^3}\right)\left(\frac{1}{4\ln\zeta}\right). \tag{A 7}$$

Appendix B. Linearized governing equations

Continuity equation:

$$\frac{1}{r}\frac{\mathrm{d}(r\hat{u}_r)}{\mathrm{d}r} + \mathrm{i}\alpha\hat{u}_z = 0. \tag{B 1}$$

Radial (r) momentum equation:

$$Re\left[\sigma\hat{u}_r - 2\frac{u_{\theta ss}\hat{u}_\theta}{r}\right] = -\frac{\partial\hat{p}}{\partial r} + \mathrm{e}^{\varepsilon(1/T_{ss}-1)} \times \left[\underbrace{\left(-\frac{\varepsilon}{T_{ss}^2}\right)\frac{\partial T_{ss}}{\partial r}\left(2\frac{\partial\hat{u}_r}{\partial r}\right)}_{\mathrm{V}} - \frac{\hat{u}_r}{r^2} + \frac{1}{r}\frac{\partial\hat{u}_r}{\partial r} + \frac{\partial^2\hat{u}_r}{\partial r^2} - \alpha^2\hat{u}_r\right]. \tag{B 2}$$

Azimuthal (θ) momentum equation:

$$\begin{aligned} Re\left[\sigma\hat{u}_\theta + \hat{u}_r\frac{\partial u_{\theta ss}}{\partial r} + \hat{u}_r\frac{u_{\theta ss}}{r}\right] &= \mathrm{e}^{\varepsilon(1/T_{ss}-1)}\left[\underbrace{-\frac{\varepsilon}{T_{ss}^2}\frac{\partial T_{ss}}{\partial r}\left(\frac{\partial\hat{u}_\theta}{\partial r} - \frac{\hat{u}_\theta}{r}\right)}_{\mathrm{V}} + \underbrace{\left(2\frac{\varepsilon}{T_{ss}^3}\right)\frac{\partial T_{ss}}{\partial r}\hat{T}\left(\frac{\partial u_{\theta ss}}{\partial r} - \frac{u_{\theta ss}}{r}\right)}_{\mathrm{VI}}\right. \\ &+ \underbrace{\left(-\frac{\varepsilon}{T_{ss}^2}\right)^2\frac{\partial T_{ss}}{\partial r}\left(\frac{\partial u_{\theta ss}}{\partial r} - \frac{u_{\theta ss}}{r}\right)\hat{T}}_{\mathrm{VI}} + \underbrace{\left(-\frac{\varepsilon}{T_{ss}^2}\right)\frac{\partial\hat{T}}{\partial r}\left(\frac{\partial u_{\theta ss}}{\partial r} - \frac{u_{\theta ss}}{r}\right)}_{\mathrm{IV}} - \frac{\hat{u}_\theta}{r^2} \\ &+ \left.\frac{1}{r}\frac{\partial\hat{u}_\theta}{\partial r} + \frac{\partial^2\hat{u}_\theta}{\partial r^2} - \alpha^2\hat{u}_\theta + \underbrace{\left(-\frac{\varepsilon}{T_{ss}^2}\right)\left(-\frac{u_{\theta ss}}{r^2} + \frac{1}{r}\frac{\partial u_{\theta ss}}{\partial r} + \frac{\partial^2 u_{\theta ss}}{\partial r^2}\right)\hat{T}}_{\mathrm{III}}\right]. \end{aligned} \tag{B 3}$$

Axial (z) momentum equation:

$$Re\,\sigma\hat{u}_z = -\mathrm{i}\alpha\hat{p} + \mathrm{e}^{\varepsilon(1/T_{ss}-1)}\left[\underbrace{\left(-\frac{\varepsilon}{T_{ss}^2}\right)\frac{\partial T_{ss}}{\partial r}\left(\frac{\partial\hat{u}_z}{\partial r} + \mathrm{i}\alpha\hat{u}_r\right)}_{\mathrm{V}} + \frac{1}{r}\frac{\partial\hat{u}_z}{\partial r} + \frac{\partial^2\hat{u}_z}{\partial r^2} - \alpha^2\hat{u}_z\right]. \tag{B 4}$$

Energy equation:

$$\sigma\hat{T} + \underbrace{\hat{u}_r \frac{\partial T_{ss}}{\partial r}}_{\text{I}} = \frac{1}{Pe}\left[\frac{\partial^2\hat{T}}{\partial r^2} + \frac{1}{r}\frac{\partial\hat{T}}{\partial r} - \alpha^2\hat{T}\right] + \underbrace{\frac{Br}{Pe}\,\mathrm{e}^{\varepsilon(1/T_{ss}-1)}\left[2\left(\frac{\partial u_{\theta ss}}{\partial r} - \frac{u_{\theta ss}}{r}\right)\left(\frac{\partial\hat{u}_\theta}{\partial r} - \frac{\hat{u}_\theta}{r}\right) + \left(-\frac{\varepsilon}{T_{ss}^2}\right) + \left(\left(\frac{\partial u_{\theta ss}}{\partial r}\right)^2 + \left(-\frac{u_{\theta ss}}{r}\right)^2 - 2\frac{\partial u_{\theta ss}}{\partial r}\frac{u_{\theta ss}}{r}\right)\hat{T}\right]}_{\text{II}}. \quad \text{(B 5)}$$

Appendix C. Derivation of scaling laws

Since the terms containing Br/Pe are negligible ($Br/Pe \ll 1$), the linearized energy equation can be reduced to the form

$$\frac{1}{Pe}\frac{\mathrm{d}^2\hat{T}}{\mathrm{d}r^2} - \left(\frac{\alpha^2}{Pe} + \sigma\right)\hat{T} = \hat{u}_r\frac{\mathrm{d}T_{ss}}{\mathrm{d}r}, \quad \text{(C 1)}$$

where $R_1/\mathrm{d} \leqslant r \leqslant R_2/\mathrm{d}$. Note that r is $O(\bar{R}/d)$ where $\bar{R} = (R_1 + R_2)/2$ or $1/r$ is $O(\delta)$. Furthermore, Δr is $O(1)$ and α^2 is $O(10)$. Hence,

$$\alpha^2\hat{u}_r \gg \frac{\mathrm{d}^2\hat{u}_r}{\mathrm{d}r^2}. \quad \text{(C 2)}$$

For a stationary mode of disturbance at the critical point, $\sigma = 0$. Also $1/Pe \to 0$, and hence, equation (C 1) reduces to

$$\hat{T} = -\frac{Pe}{\alpha^2}\frac{\mathrm{d}T^{ss}}{\mathrm{d}r}\hat{u}_r. \quad \text{(C 3)}$$

Alternatively, if one treats the right-hand side of equation (C 1) as a source term, then since $\hat{T} = 0$ at $r = R_1/d$ and R_2/d, the homogeneous solution to (C 1) is identically zero when $\sigma = 0$. This leads to equation (C 3).

In the momentum equation, we make the approximation $\exp(\varepsilon(1/T_{ss} - 1)) \approx 1$ since the maximum dimensionless temperature difference is $O(1/T_1^*)$. In addition, we neglect term V in equation (B 2) as it has very little influence on the critical conditions: see § 3.3. Invoking the narrow-gap approximation, equation (B 2) can be reduced to

$$Re\left[\sigma + \frac{\alpha^2}{Re}\right]\hat{u}_r = \frac{2Re}{r}u_{\theta ss}\hat{u}_\theta - \frac{\mathrm{d}\hat{p}}{\mathrm{d}r}. \quad \text{(C 4)}$$

Similar approximations when applied to equation (B 4) result in

$$Re\,\sigma\hat{u}_z = -\mathrm{i}\alpha\hat{p} - \alpha^2\hat{u}_z, \quad \text{(C 5)}$$

which upon re-arrangement of the terms gives

$$\hat{p} = \frac{\mathrm{i}Re}{\alpha}\left[\sigma + \frac{\alpha^2}{Re}\right]\hat{u}_z. \quad \text{(C 6)}$$

At the critical point, i.e. when $\sigma = 0$, equation (C 6) becomes

$$\hat{p} = \mathrm{i}\alpha\hat{u}_z. \quad \text{(C 7)}$$

In the narrow-gap limit, the continuity equation (B 1) reduces to

$$\mathrm{i}\alpha\hat{u}_z = \frac{\mathrm{d}\hat{u}_r}{\mathrm{d}r}. \tag{C 8}$$

Using equations (C 7) and (C 8) in (C 4), we obtain

$$\frac{\mathrm{d}^2\hat{u}_r}{\mathrm{d}r^2} + Re\left[\sigma + \frac{\alpha^2}{Re}\right]\hat{u}_r = \frac{2Re}{r}u_{\theta ss}\hat{u}_\theta. \tag{C 9}$$

In order to eliminate $\hat{u}_\theta$ from equation (C 9), we make use of the linearized θ-momentum equation (B 3) (terms V and VI have been neglected as they have very little influence on the critical condition: see § 3.3), i.e.

$$Re\left[\sigma + \frac{\alpha^2}{Re}\right]\hat{u}_\theta + Re\frac{\mathrm{d}u_{\theta ss}}{\mathrm{d}r}\hat{u}_r = -\frac{\varepsilon}{T_{ss}^2}\left[\frac{\mathrm{d}\hat{T}}{\mathrm{d}r}\frac{\mathrm{d}u_{\theta ss}}{\mathrm{d}r} + \hat{T}\frac{\mathrm{d}^2u_{\theta ss}}{\mathrm{d}r^2}\right]. \tag{C 10}$$

Substituting for $\hat{T}$ from (C 3) in (C 10), gives

$$Re\left[\sigma + \frac{\alpha^2}{Re}\right]\hat{u}_\theta = -Re\frac{\mathrm{d}u_{\theta ss}}{\mathrm{d}r}\hat{u}_r + \frac{\varepsilon}{T_{ss}^2}\frac{Pe}{\alpha^2}\frac{\mathrm{d}T_{ss}}{\mathrm{d}r}\left[\frac{\mathrm{d}u_{\theta ss}}{\mathrm{d}r}\frac{\mathrm{d}\hat{u}_r}{\mathrm{d}r} + \frac{\mathrm{d}^2u_{\theta ss}}{\mathrm{d}r^2}\hat{u}_r\right]. \tag{C 11}$$

Let $K \equiv \varepsilon Pe/(T_{ss}\alpha)^2$, $\Theta' \equiv \mathrm{d}T_{ss}/\mathrm{d}r$, $U \equiv u_{\theta ss}$, $U' \equiv u'_{\theta ss}$ and $U'' \equiv u''_{\theta ss}$ so that equation (C 11) for a stationary mode of disturbance can be re-written succinctly as

$$\alpha^2\hat{u}_\theta = -ReU'\hat{u}_r + K\Theta'\left[U'\frac{\mathrm{d}\hat{u}_r}{\mathrm{d}r} + U''\hat{u}_r\right]. \tag{C 12}$$

Using (C 12) in (C 9) and letting $\sigma = 0$ (at critical point), we get a simplified master equation for Dean and Taylor–Couette flows:

$$\frac{\mathrm{d}^2\hat{u}_r}{\mathrm{d}r^2} + \left[\alpha^2 + \frac{2ReUU'}{\alpha^2 r}\right]\hat{u}_r = \frac{2ReUK\Theta'}{\alpha^2 r}\left[U'\frac{\mathrm{d}\hat{u}_r}{\mathrm{d}r} + U''\hat{u}_r\right]. \tag{C 13}$$

Equation (C 13) is a second-order eigenvalue problem closed in $\hat{u}_r$ with homogeneous Dirchlet boundary conditions at the cylinder walls. Note that the analytical results for the steady-state velocity and temperature gradient presented in § 3.1 can be used in equation (C 13). We seek a power series solution for $\hat{u}_r$ as

$$\hat{u}_r = \sum_{n=1}^{\infty} a_n x^n, \tag{C 14}$$

where $x = r - r_1$, $0 \leqslant x \leqslant 1$. Note that $a_0 = 0$ by virtue of the boundary condition at $x = 0$. In the following subsections, we present the derivation of the scaling law for Taylor–Couette and Dean flows respectively.

C.1. *Taylor–Couette flow*

Re-writing equation (C 13) in terms of x and re-arranging gives

$$\alpha^2 x\frac{\mathrm{d}^2\hat{u}_r}{\mathrm{d}x^2} + \alpha^2 r_1\frac{\mathrm{d}^2\hat{u}_r}{\mathrm{d}x^2} + [\alpha^4 x + \alpha^4 r_1 + 2Re^2UU']\hat{u}_r = 2ReUK\Theta'\left[U'\frac{\mathrm{d}\hat{u}_r}{\mathrm{d}x} + U''\hat{u}_r\right]. \tag{C 15}$$

In the narrow-gap limit, the steady-state variables can be written as $U = 1 - x$ and $\Theta' = S + c_1 Na$ where c_1 is assumed to be a constant for sake of simplicity.

Substituting equation (C 14) in (C 15), we obtain

$$\alpha^2 \sum_{n=-1}^{\infty} a_{n+2}(n+2)(n+1)x^{n+1} + \alpha^2 r_1 \sum_{n=-2}^{\infty} a_{n+3}(n+3)(n+2)x^{n+1} + \alpha^4 \sum_{n=1}^{\infty} a_n x^{n+1} + \alpha^4 r_1 \sum_{n=0}^{\infty} a_{n+1}x^{n+1} + 2Re^2 \sum_{n=1}^{\infty} a_n x^{n+1} - 2Re^2 \sum_{n=0}^{\infty} a_{n+1}x^{n+1} = 2ReK\Theta' \sum_{n=1}^{\infty} a_n x^{n+1} - 2ReK\Theta' \sum_{n=0}^{\infty} a_{n+1}x^{n+1}. \quad (C\,16)$$

Collecting the coefficients of like powers of x, we get

$$x^0 : 2\alpha^2 r_1 a_2 = 0, \quad \text{i.e. } a_2 = 0, \quad (C\,17)$$

$$x^1 : (\alpha^4 r_1 - 2Re^2 + 2Re\,K\Theta')a_1 + 6\alpha^2 r_1 a_3 = 0, \quad (C\,18)$$

$$x^2 : (\alpha^4 + 2Re^2 - 2Re\,K\Theta')a_1 + 6\alpha^2 a_3 + 12\alpha^2 r_1 a_4 = 0, \quad (C\,19)$$

$$x^3 : (\alpha^4 r_1 - 2Re^2 + 2Re\,K\Theta')a_3 + 12\alpha^2 a_4 = 0. \quad (C\,20)$$

The series expression in (C 14) is truncated to a cubic expression in x. Equations (C 18)–(C 20) constitute a homogeneous set of linear equations. Therefore, in order to obtain a non-trivial solution for the coefficients a_1, a_3 and a_4, it is required by Fredholm's alternative that the determinant of the coefficient matrix must be equal to zero, i.e.

$$\begin{vmatrix} \alpha^4 r_1 - 2Re^2 + 2Re\,K\Theta' & 6\alpha^2 r_1 & 0 \\ \alpha^4 + 2Re^2 - 2Re\,K\Theta' & 6\alpha^2 & 12\alpha^2 r_1 \\ 0 & \alpha^4 r_1 - 2Re^2 + 2Re\,K\Theta' & 12\alpha^4 \end{vmatrix} = 0. \quad (C\,21)$$

After substituting $r_1 = 1/\delta$, $K = \varepsilon Pe/(T_{ss}\alpha)^2$ and $\Theta' = S + c_1 Na$ in (C 21), the determinant can be reduced to an expression of the form

$$Re_c \delta^{1/2} = \sqrt{\frac{12\alpha^6 - \delta}{24\alpha^2}} \Big/ \left[1 - \frac{Pr}{T_{ss}^2 \alpha^2}(S + c_1 Na)\right]^{1/2}. \quad (C\,22)$$

Using the fact that $\delta \ll 12\alpha^6$, and in the isothermal limit, equation (C 22) simplifies to the form

$$Re_c \delta^{1/2} = \alpha/\sqrt{2} = \text{a constant}. \quad (C\,23)$$

Although the constant is not equal to 41 (Taylor 1923) due to the approximations involved in the derivation, expression (C 23) conforms to the isothermal critical condition $Re_{c,iso}\delta^{1/2} = $ a constant. Moreover, our interest is in predicting the relative destabilization characterized by the ratio of the critical Reynolds numbers for the non-isothermal and isothermal flows, i.e. Λ. Using equations (C 22) and (C 23), it can be shown that

$$\Lambda = \frac{1}{\left[1 - \left(Pr/T_{ss}^2\alpha^2\right)(S + c_1 Na)\right]^{1/2}}. \quad (C\,24)$$

C.2. *Dean flow*

The series expression for $\hat{u}_r$ from (C 14) is substituted in the master equation (C 15), where in the narrow-gap limit, the steady-state variables can be approximately written

as $U = x(1-x)$ and $\Theta' = S + c_2 Na$ where c_2 is a constant, i.e. given by

$$\alpha^2 \sum_{n=-3}^{\infty} a_{n+4}(n+4)(n+3)x^{n+3} + \frac{\alpha^2}{\delta} \sum_{n=-4}^{\infty} a_{n+5}(n+5)(n+4)x^{n+3} + \alpha^4 \sum_{n=-1}^{\infty} a_{n+2}x^{n+3}$$
$$+ \frac{\alpha^4}{\delta} \sum_{n=-2}^{\infty} a_{n+3}x^{n+3} + 4Re^2 \sum_{n=1}^{\infty} a_n x^{n+3} - 6Re^2 \sum_{n=0}^{\infty} a_{n+1}x^{n+3} + 2Re^2 \sum_{n=-1}^{\infty} a_{n+2}x^{n+3}$$
$$= 2Re\, K\Theta' \left[2\sum_{n=0}^{\infty} a_{n+1}(n+1)x^{n+3} - 3\sum_{n=-1}^{\infty} a_{n+2}(n+2)x^{n+3} + \sum_{n=-2}^{\infty} a_{n+3}(n+3)x^{n+3} \right.$$
$$\left. - 2\sum_{n=-1}^{\infty} a_{n+2}x^{n+3} + 2\sum_{n=0}^{\infty} a_{n+1}x^{n+3} \right] \tag{C 25}$$

Collecting the coefficients of like powers of x, we get

$$x^0 : 2\alpha^2 r_1 a_2 = 0, \quad \text{i.e. } a_2 = 0, \tag{C 26}$$
$$x^1 : (\alpha^4 r_1 - 2Re\, K\Theta')a_1 + 6\alpha^2 r_1 a_3 = 0, \tag{C 27}$$
$$x^2 : (\alpha^4 + 2Re^2 + 10Re\, K\Theta')a_1 + 6\alpha^2 a_3 + 12\alpha^2 r_1 a_4 = 0, \tag{C 28}$$
$$x^3 : (-6Re^2 - 8Re\, K\Theta')a_1 + (\alpha^4 r_1 - 6Re\, K\Theta')a_3 + 12\alpha^2 a_4 = 0. \tag{C 29}$$

Once again, we truncate the series at the cubic term. Equations (C 27)–(C 29) constitute a homogeneous set of linear equations. Therefore, the existence of non-trivial solutions is guaranteed only if

$$\begin{vmatrix} \alpha^4 r_1 - 2Re\, K\Theta' & 6\alpha^2 r_1 & 0 \\ \alpha^4 + 2Re^2 + 10Re\, K\Theta' & 6\alpha^2 & 12\alpha^2 r_1 \\ -6Re^2 - 8Re\, K\Theta' & \alpha^4 r_1 - 6Re\, K\Theta' & 12\alpha^4 \end{vmatrix} = 0. \tag{C 30}$$

After substituting $r_1 = 1/\delta$, $K = \varepsilon Pe/(T_{ss}\alpha)^2$ and $\Theta' = S + c_2 Na$ in (C 30) and through similar procedure as followed for the Taylor–Couette flow, it can be shown that

$$\Lambda = \frac{1}{\left[1 - \left(c_3 Pr/T_{ss}^2\alpha^2\right)(S + c_2 Na)\right]^{1/2}}, \tag{C 31}$$

where c_3 is a constant. The numerical values of c_2 and c_3 will be determined by fitting the above expression to numerical linear stability analysis results: see § 3.4.

REFERENCES

Al-Mubaiyedh, U. A., Sureshkumar, R. & Khomami, B. 1999 Influence of energetics on the stability of viscoelastic Taylor–Couette flow. *Phys. Fluids* **11**, 3217.

Al-Mubaiyedh, U. A., Sureshkumar, R. & Khomami, B. 2002 The effect of viscous heating on the stability of Taylor–Couette flow. *J. Fluid Mech.* **462**, 111.

Bird, R. B., Armstrong, R. C. & Hassager, O. 1987 *Dynamics of Polymeric Liquids*. Vol. 1, 2nd Edn. John Wiley and Sons.

Chandrasekhar, S. 1961 *Hydrodynamic and Hydrodynamic Stability*. Dover.

Dean, W. R. 1928 Fluid motion in a curved channel. *Proc. R. Soc. Lond.* A **121**, 402.

Papathanasiou, T. D. 1997 Circular Couette flow of temperature-dependent materials: asymptotic solutions in the presence of viscous heating. *Chem. Engng Sci.* **52**(12), 2003.

Pearson, J. R. A. 1978 Polymer flows dominated by high heat generation and low heat transfer. *Polymer Engng Sci.* **18**(3), 222.

Taylor, G. I. 1923 Stability of a viscous liquid contained between rotating cylinders. *Phils. Trans. R. Soc. Lond.* A **223**, 289.

Thomas, D. G., Sureshkumar, R. & Khomami, B. 2003 Influence of fluid thermal sensitivity on the thermo-mechanical stability of the Taylor–Couette flow. *Phys. Fluids* **15**, 3308.

Turian, R. F. 1965 Viscous heating in the cone-and-plate viscometer. Non-Newtonian fluids with temperature-dependent viscosity and thermal conductivity. *Chem. Engng Sci.* **20**, 771.

White, J. M. & Muller, S. J. 2000 Viscous Heating and the stability of Newtonian and Viscoelastic Taylor–Couette flows. *Phys. Rev. Lett.* **84**, 5130.

White, J. M. & Muller, S. J. 2002*a* Experimental studies on the stability of Newtonian Taylor–Couette flow in the presence of viscous heating. *J. Fluid Mech.* **462**, 133.

White, J. M. & Muller, S. J. 2002*b* The role of thermal sensitivity of fluid properties, centrifugal destabilization, and nonlinear disturbances on the viscous heating instability in Newtonian Taylor–Couette flow. *Phys. Fluids* **14**, 3880.